R-04-04

Äspö Pillar Stability Experiment

Modelling of fracture development of APSE by FRACOD

Mikael Rinne, Baotang Shen, Hee-Suk Lee
Fracom Ltd

March 2004

Svensk Kärnbränslehantering AB
Swedish Nuclear Fuel
and Waste Management Co
Box 5864
SE-102 40 Stockholm Sweden
Tel 08-459 84 00
+46 8 459 84 00
Fax 08-661 57 19
+46 8 661 57 19

ISSN 1402-3091
SKB Rapport R-04-04

Äspö Pillar Stability Experiment

Modelling of fracture development of APSE by FRACOD

Mikael Rinne, Baotang Shen, Hee-Suk Lee
Fracom Ltd

March 2004

Keywords: Fracture initiation, Fracture propagation, Spalling, AE.

Abstract

An in-situ experiment has started at Äspö HRL to investigate the stability of a pillar between two closely located boreholes of deposition hole scale. This full-scale experiment is named the Äspö Pillar Stability Experiment (APSE).

One of the holes will be pressurized with 0.8 MPa water pressure to simulate confinement by backfill. Thermal stresses will be applied in the pillar by the use of electric heaters to reach the spalling conditions. To quantify the degree of damage during the experiment, an Acoustic Emission (AE) system will be used and strain measurements will be installed.

FRACOD is a two dimensional BEM/DDM code for fracturing analysis in rock material. Here it has been used to model the rock mass response during the planned sequences of excavation-confinement-heating. The models predict the stress and displacement fields, fracture initiation and propagation, coalescence and the final failure of the rock mass. The presences of pre-existing fractures, which may have significant influence on the pillar behaviour, have also been considered in the modelling. This report summarises the modelling work using FRACOD to simulate the various experimental stages.

Sammanfattning

Ett insitu experiment har påbörjats vid Äspö HRL vilket skall undersöka stabiliteten av en bergpelare mellan två tätt borrade borrhål i deponeringshålsskala. Fullskaleförsöket är benämnt Äspö Pillar Stability Experiment (APSE).

Ett av borrhålen kommer att trycksättas med ett vattentryck på 0,8 MPa för att simulera backfillens svälltryck. Termiska laster kommer att läggas på pelaren genom elektriska värmare för att uppnå den last som krävs för att sprött brott skall initieras. För att kvantifiera graden av de spröda brotten under experimentet kommer ett akustiskt system att tillsammans med deformationsmätningar att användas för moneteringen.

FRACOD är en tvådimensionell BEM/DDM kod för analys av sprickbildning i berg-material. I detta försök har FRACOD använts för att modellera bergmassans respons under de planerade experimentsekvenserna som består av bergarbeten-trycksättning-värmning. Modellerna ger prediktioner på spännings och deformationsfält, sprickinitiering och propagering, föreningen av de propagerande sprickorna samt det slutliga brottet i bergmassan. Förekomsten av befintliga sprickor i experimentvolymen, vilka kraftigt kan påverka pelarens uppträdande vid belastning, har beaktats vid modelleringen. Denna rapport sammanfattar det modellarbete som genomförts med FRACOD för att simulera de olika delarna av experimentet.

Contents

1 Overview of the APSE project

1.1 Introduction

An in-situ experiment has been commenced at Äspö HRL to investigate the stability of a pillar between two closely located deposition holes. This full-scale experiment is named the Äspö Pillar Stability Experiment (APSE). The experiment requires a new tunnel that is excavated at the 450 m level. In the tunnel two large holes with a diameter of 1.8 m and a depth of 8.0 m will be bored. The holes will be spaced to create a pillar with the width of 1.0 m between them. The tunnel will be designed to induce the stresses in the pillar to a level close to the limit of spalling (Figure 1-1). Electric heaters will be used to induce thermal stresses in the pillar that would force the rock in the pillar walls to spall. To simulate the effect of confinement from backfill in real deposition hole, a water pressure of 0.8 MPa will be applied in one of the holes. The effect of the confining pressure will be further studied by gradually releasing it. The whole experimental stages will be monitored by an acoustic emission (AE) and micro-seismic system. Convergence and strain measurements will also be made in the open hole to control the rock mass behaviour around the boreholes.

The modelling includes the planned steps of excavation-confinement-heating sequence to predict the degree of spalling and fracturing stress and displacement fields together with temperature fields in the pillar region. Preliminary modelling was carried out before excavation of the research tunnel. Numerical models with Examine3D, FLAC3D, JobFem and FRACOD have been reported by the modelling teams during the spring 2003.
A summary of the experiment and the preliminary modelling work have been reported in two conference papers of the GeoProc 2003 by /Andersson et al. 2003/ and by /Rinne et al. 2003b/.

FRACOD is a boundary element code for fracture stability analysis in rock material /Shen B, 2002/. It has been developed to model fracturing process of the rock material in varying loading conditions. For the APSE project, FRACOD has been updated in many respects including AE simulation. A method to import stresses from other numerical models to FRACOD has also been developed. The preliminary models as well as the updated code have been presented in /Rinne et al. 2003a/.

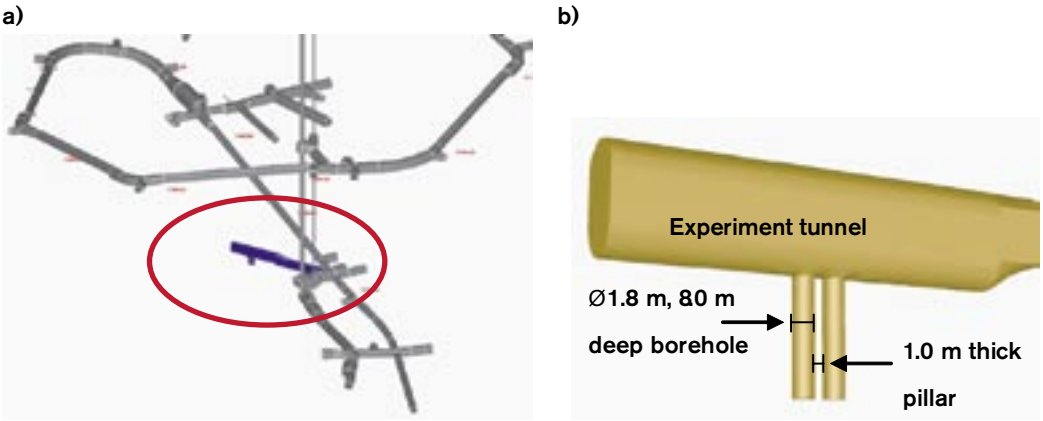

Figure 1-1. *(a) APSE experiment tunnel at 450 m depth. (b) General layout of the experiment with a 1.0 m thick pillar between two 1.8 m diameter and 8.0 m deep boreholes. The tunnel is oriented perpendicular to the maximum principal in-situ stress, σ_1. /Andersson et al. 2003/.*

Additional field data has been received following the previous modelling study. Laboratory investigations have been reported by /Backers, 2003/ and /Kuula, 2003/ in /Staub et al. 2004/. In addition, site investigations have been reported /Barton, 2003/. This report summarizes the outcomes of FRACOD modelling with updated input parameters. A new stress model has been reconstructed and additional calculations have been conducted to estimate parameter sensitivity and the effect of pre-existing fractures. The sensitivity analysis and the updated stress reconstruction are presented in Appendix 1 and 2.

1.2 Objectives

The objectives of this experiment are:

1) To demonstrate the capability to predict brittle failure (spalling) in a fractured rock mass,
2) to demonstrate the effect of backfill (confining pressure) on the brittle failure response and
3) to compare 2D and 3D mechanical and thermal numerical predicting capabilities.

Two key components of the FRACOD modelling work are:

1) To predict properly the fracturing process during the planned sequences of excavation-confinement-heating and
2) to develop and demonstrate the capacity of FRACOD in predicting Acoustic Emission (AE) during the progressive fracturing process in the pillar.

1.3 Excavation and loading steps

The description of the planned experiment, instrumentation and the results of preliminary numerical calculations are reported in /Andersson, 2003/ and in /Fredriksson et al. 2003/. These reports present the layout of the experiment, with the locations of the AE monitoring sensors, the heaters and the temperature measurement points during the experiment. Different locations of the heaters have been analysed. Figure 1-2 resents the proposed layout of acoustic emission system and the heaters.

The main APSE excavation and loading steps are as follows:

(a) Excavation of a test tunnel, 5.0 m by 7.5 m in size, with an inverse floor arch at 450 m below ground surface.

(b) Installation of AE transducers.

(c) Drilling of the first deposition hole of 1.8 m in diameter, 8.0 m in depth.

(d) Pressuring the first hole with watertight membrane up to 0.8 MPa to simulate the effects of swelling pressure of backfill.

(e) Drilling of the second deposition hole (1.0 m pillar thickness).

(f) Installation of instrumentation and heaters.

(g) Heating the pillar with electrical heaters installed near the two deposition holes. The heating continues until failure of the wall of the deposition hole occurs.

(h) Gradual reduction of the confining pressure in the first deposition hole until spalling occurs.

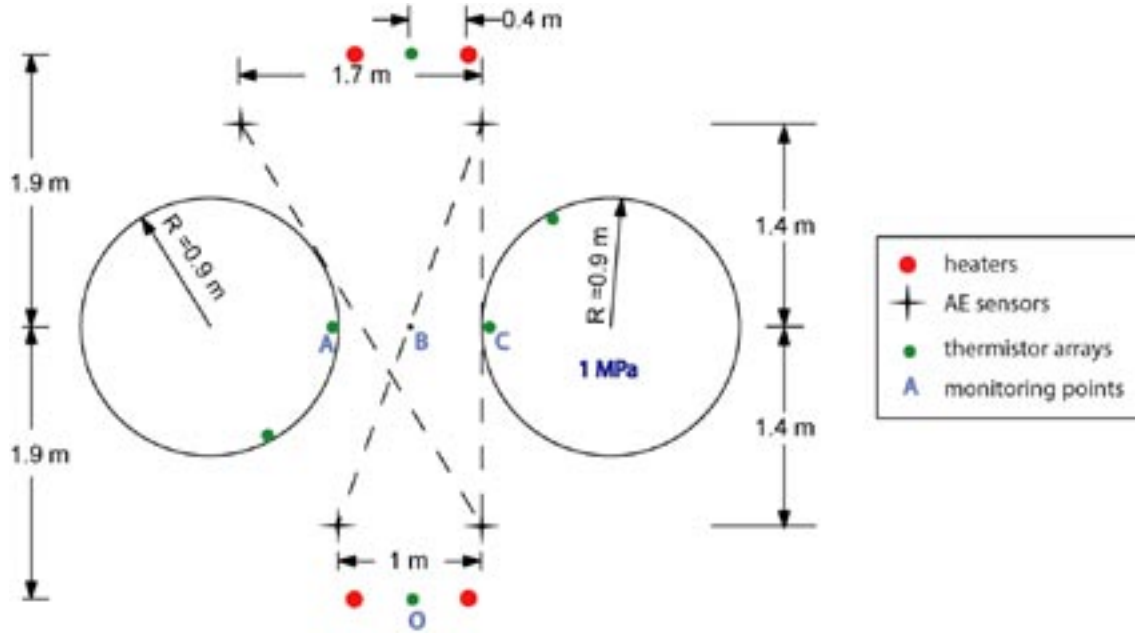

Figure 1-2. *Planned borehole geometry and instrumentations /Fredriksson et al. 2003/. Water pressure of 0.8 MPa will be applied into the borehole at right in the figure.*

2 Input parameters

2.1 Rock and fracture properties

The geology and stress data of the rock volume in the experimental area are summarized in /Staub et al. 2003/. Rock and fracture properties based on laboratory investigations by /Nordlund et al. 1999/, /Klee et al. 2001/ and /Staub et al. 2004/ have been considered in evaluation of input parameters. The input parameter has been evaluated in /Rinne et al. 2003a/ and in the sensitivity analysis presented in Appendix 1. The rock material is assumed to be homogeneous, isotropic and linear elastic. Barton-Bandis model has been applied to estimate the fracture properties for new initiated fractures /Barton, 1986/ and /Bandis et al. 1983/. The mathematical treatment of input data in FRACOD has been described in /Rinne et al. 2003a/.

Table 2-1. Input data for FRACOD models.

Parameter	Value and unit
Rock mass	
Young's modulus	55 GPa
Poisson's ratio	0.26
Cohesion *	31 MPa
Friction angle *	49°
Tensile strength	14.3 MPa
Fractures	
Fracture toughness in mode I	3.80 MPa $m^{1/2}$
Fracture toughness in mode II	6.35 MPa $m^{1/2}$
Properties of new shear fractures	
Fracture stiffness: K_n and K_s	26,976 (GPa/m)
Friction angle	49.0 (°)
Cohesion	31 (MPa), 0 after sliding
Dilation angle	2.3 (°)
Properties of new tensile fractures	
Fracture stiffness: K_n and K_s	26,976 (GPa/m)
Friction angle	49.0 (°)
Cohesion	31 (MPa), 0 after sliding
Dilation angle	12.1 (°)

* Uniaxial compressive strength is 166 MPa, according to Mohr-Coloumb failure criterion. See Appendix 1.

2.2 Stress conditions

A summary of in-situ stresses in the experiment area have been presented in /Staub et al. 2003/. The most probable value of major stress in the experimental volume is estimated as:

Table 2-2. In-situ stresses in the experimental rock volume.

σ_1 [MPa]	σ_2 [MPa]	σ_3 [MPa]	Trend [Äspö 96]	Dip
27			310	07
	15		090	83
		10	208	00

2.3 Stress models

The stress analysis of the experiment area has been described in /Andersson, 2003/ and /Fredriksson et al. 2003/. A feasibility study for performing the APSE has been reported by SKB /Andersson, 2003/ to identify risks and to describe the strategy for the modelling. In this study the stress redistribution caused by tunnel and borehole excavation has been analysed using the boundary element code EXAMINE3D and the finite element code PHASE2D. Two horizontal cross sections (0.5 m and 1.5 m below the tunnel floor) are obtained in order to consider the difference in stress distribution due to 3D effects. Golder Associates have calculated stresses caused by heating by a 2D-coupled thermo-mechanical finite element code JobFem. Fracom Ltd performed simulation of the fracturing process using FRACOD and input data from EXAMINE3D and JobFem. Internal stresses from JobFem models were reconstructed using proper boundary stresses for the FRACOD models. The stress reconstruction has been described in /Rinne et al. 2003a, Part III/. A summary of stress reconstruction technique and the updated stress distribution is presented in Appendix 2.

Simultaneously Saanio & Riekkola has performed 3D-coupled thermo-mechanical modelling with the finite difference code FLAC3D /Wanne et al. 2004/.

The stress data-set from EXAMINE3D and JobFem modeling includes the following phases:

Stress state I: stress conditions after excavation of both boreholes (EXAMINE3D).

Stress state II: stresses after 30 days of heating (JobFem).

Stress state III: stresses after 60 days of heating (JobFem).

Stress state IV: stresses after 90 days of heating (JobFem).

Stress state V: stresses after 120 days of heating (JobFem).

The effect of 0.8 MPa hydraulic pressure in one of the boreholes has been included in the stress data and definition of thermally induced stresses by heating.

3 FRACOD pillar models

FRACOD pillar models aim to study correct and detailed stress field in the pillar between two closely excavated boreholes and to study fracture initiation and propagation in the stress field elevated by thermal loading. Two sections have been modelled, 1.5 m and 0.5 m below the tunnel floor. Due to 3-D stress distribution, the stresses are unevenly distributed in the pillar and non-symmetric models have been used.

3.1 Elastic models

The reconstructed elastic stresses (stresses without effect of fracturing) have been presented in Appendix 2. A summary of maximum compressive stresses with and without the effect of fracturing for each loading step is presented in Table 3-1.

3.2 Failure pattern

3.2.1 Section 1.5 m below the tunnel floor

Calculations suggest that the maximum compressive stress in the pillar boundary after excavation of both boreholes is about 122 MPa (see Table 3-1). Induced stress will cause some elastic fracture initiation at the borehole boundary. In practice, this slight fracturing might be difficult to distinguish from the damage caused by mechanical borehole drilling (Figure 3-1).

After applying the thermal stresses, the fracture initiation and propagation continue as stresses increase in the pillar. After 30 days of heating limited fracture propagation and coalescence are predicted to occur in the vicinity of the central borehole walls. Fracture propagation continues successively with stress increase in a limited area close the pillar wall. Possible spalling is restricted to a narrow area at the borehole boundary after 120 days of heating. The fracture propagation is stable and the pillar core will remain intact.

Table 3-1. Maximum compressive stresses (MPa) for each loading step.

Section	Excavation	Hydraulic (*) pressure	30 days	60 days	90 days	120 days
Elastic models						
1.5 m	122.5	122.1	145.3	161.7	169.5	175.8
0.5 m	140.2	139.6	162 .8	179.3	187.1	193.4
Brittle models						
1.5 m	120.6	120.2	139.0	152.6	159.9	164.8
0.5 m	134.0	133.9	153.5	167.6	174.9	181.7

* Confinement of 0.8 MPa added on one borehole boundary.

Section 1.5 m below tunnel floor

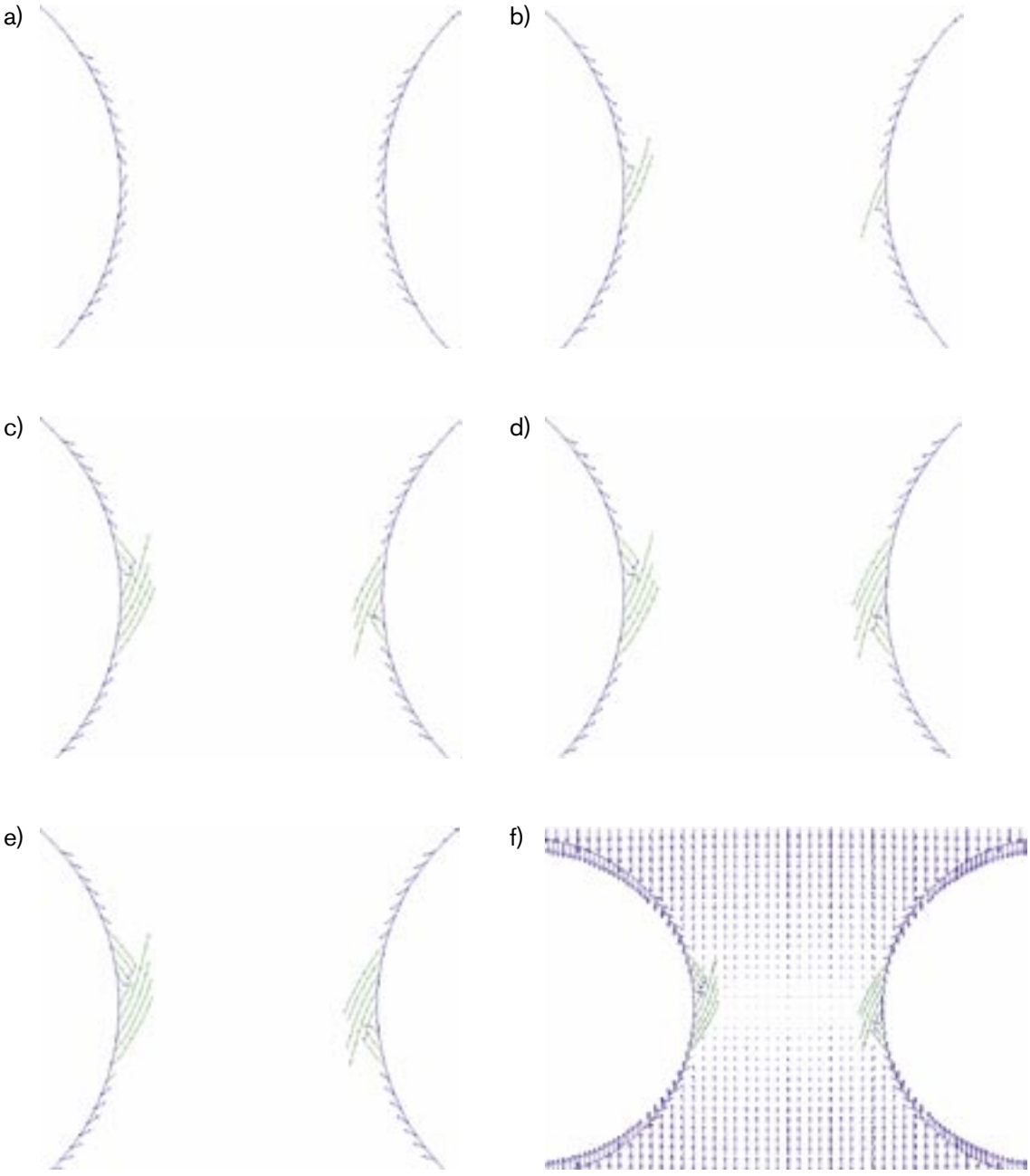

Figure 3-1. *Fracture initiation and propagation at the borehole boundary of section 1.5 m below the tunnel floor. (a) Fracture pattern after excavation. (b) After 30 days of heating. (c) After 60 days of heating. (d) After 90 days of heating. (e) After 120 days of heating. (f) Displacements after 120 days of heating. The borehole at right is pressurized by 0.8 MPa. See magnitude of displacements in Figure 3-5.*

3.2.2 Section 0.5 m below the tunnel floor

The fracture pattern in the section 0.5 m below tunnel floor after excavation is similar to that presented for section 1.5 m, but some of the initiated fractures have propagated. The maximum induced stress in the pillar boundary after excavation is about 140 MPa. After limited failure, the maximum stress at the borehole boundary will drop to 134 MPa (Figure 3-3).

Extension of fractures along the central part of the borehole walls takes place continuously with stress increase induced by heating. The intensity of fracture initiation and propagation will decrease after 90 days of heating and the fracture pattern is much like the fracture pattern after 120 days of heating.

The intact area of the pillar is slightly decreased compared to 1.5 m section after 120 days of heating. Fractures may form V-shaped shear spalled zones on both sides on the pillar boundary. In spite of quite extensive fracturing at the pillar wall, overall stability would be maintained after 120 days of heating.

Based on the stress distribution from subsequent thermal loading, overall stress level in pillar region is significantly increased compared to the stress state after excavation.

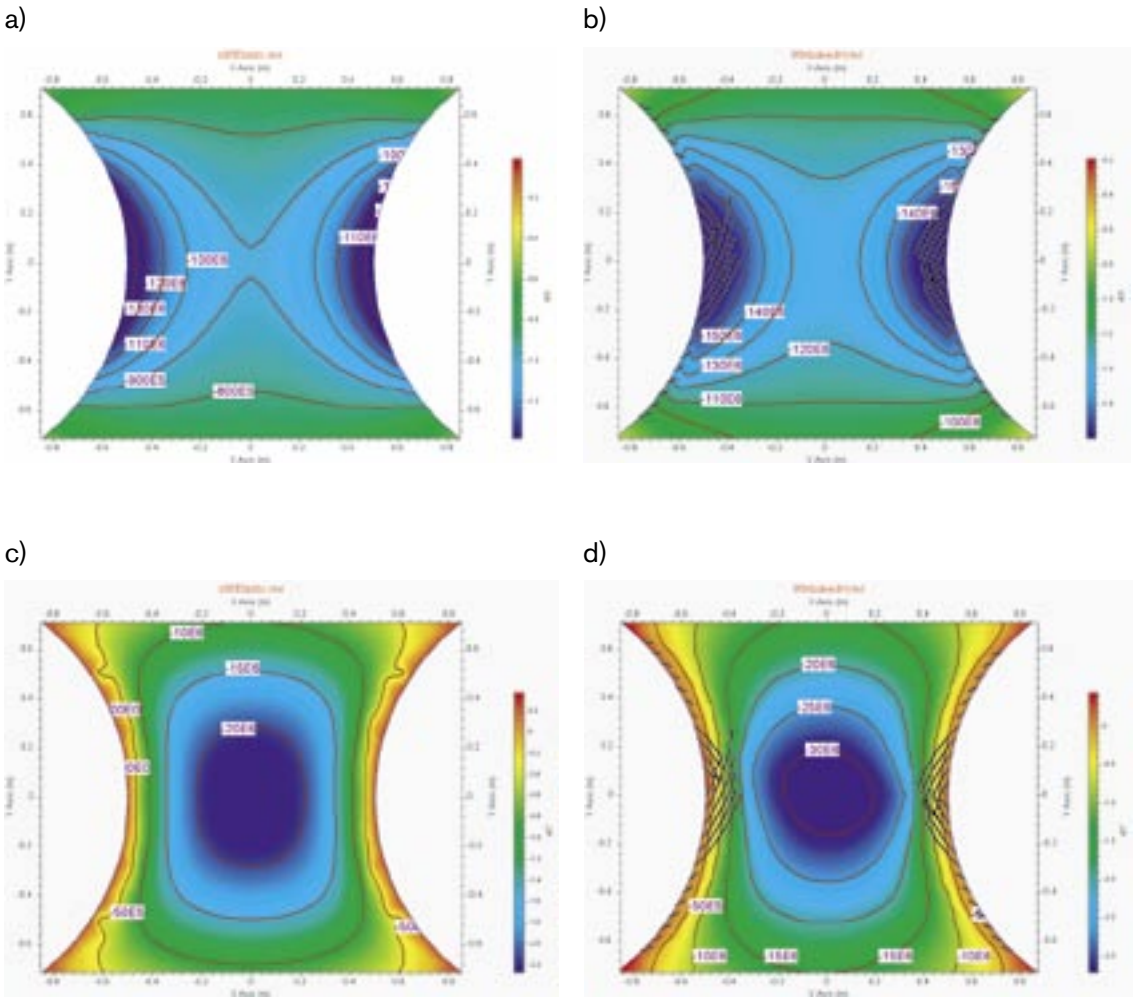

Figure 3-2. *(a) Compressive stress (σ_1) distribution caused by excavation before failure. (b) Brittle model and compressive stress after 120 days of heating. (c) Minor stress (σ_3) distribution caused by excavation before failure. (d) Brittle model and minor stress after 120 days of heating.Section 0.5 m below tunnel floor*

Section 0.5 m below tunnel floor

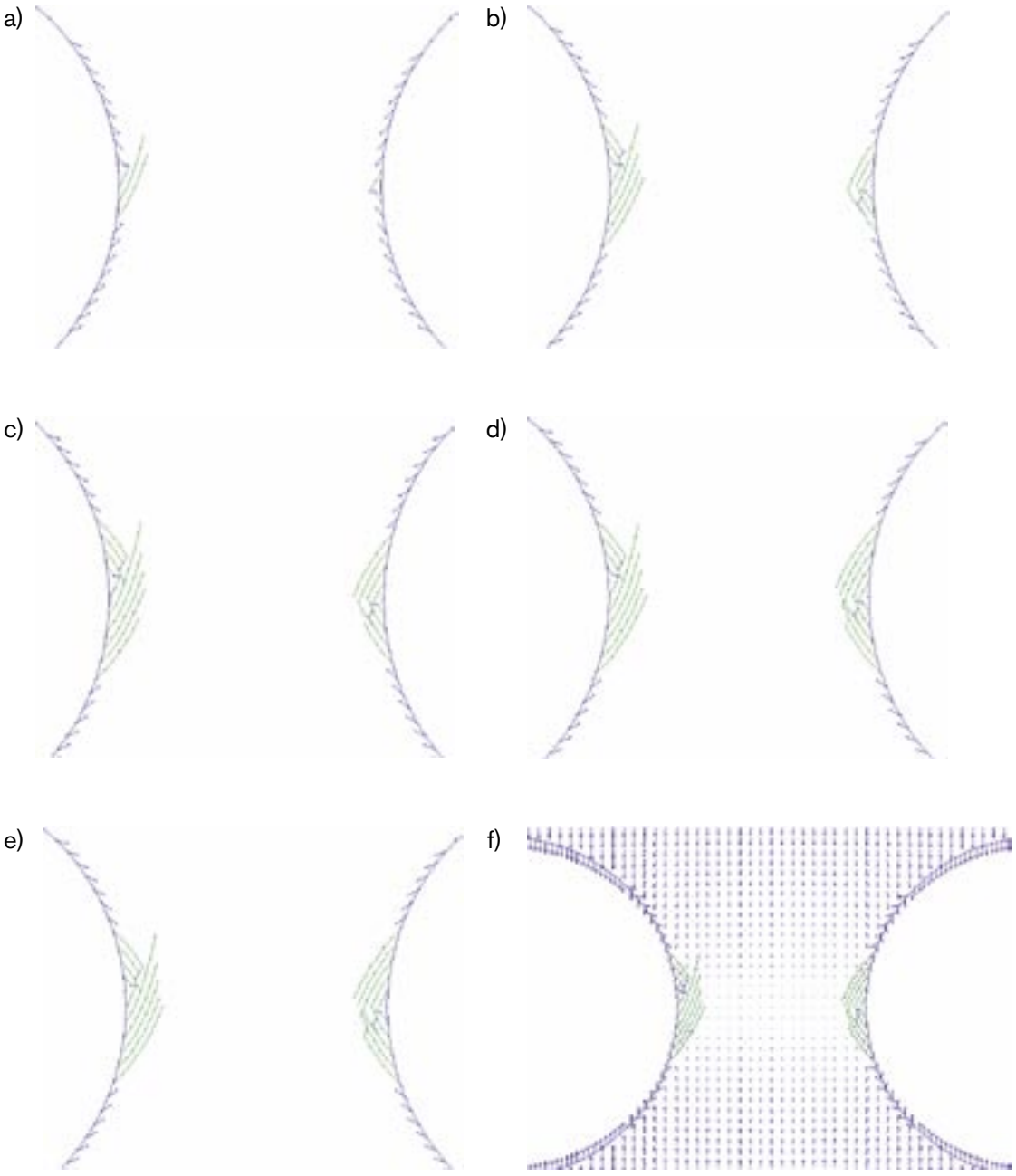

Figure 3-3. *Fracture initiation and propagation at the borehole boundary of section 0.5 m below the tunnel floor. (a) Fracture pattern after excavation. (b) After 30 days of heating. (c) After 60 days of heating. (d) After 90 days of heating. (e) After 120 days of heating. (f) Displacements after 120 days of heating. The borehole at right is pressurized by 0.8 MPa. See magnitude of displacements in Figure 3-6.*

3.3 Effect of confinement

The confining pressure from hydraulic pressurisation was only included in the imported heating data set but not in the original excavation data set. The confinement must be taken into account before applying heating induced stresses to produce correct initial fracture pattern prior to heating. For FRACOD models the 0.8 MPa hydraulic confinement has been added in the excavation stress data as a boundary stress on the borehole wall. By introducing the confinement as a boundary stress we also avoid possible inaccuracies in the imported reconstructed stress data. The confinement, however, is less than one percent of the major compressive stress in the critical pillar section. Small inaccuracies in stress reconstruction may smooth out the confining effect on the boundary. As a consequence of this, the confining pressure of 0.8 MPa has been applied twice during the heating phase, because the confinement could not be subtracted from the heating data. However, simulation with single confinement (only included in the heating stress data) results in very similar stress distribution compared to the stresses with double confinement. Some difference can be detected on the fracture patterns, but the overall effect is not remarkable.

Fracture growth and AE activity at the right pillar boundary is reduced compared to the left side. The effect of confinement is more pronounced before 90 days of heating for both 0.5 m and 1.5 m sections.

After 120 days of heating there are 56 fracture elements on the left side and 50 elements on the confined side in the section 1.5 m below tunnel floor. In section 0.5 m there are 67 fracture elements on the left side and on the confined side 56 elements, respectively. The calculation suggests that fracture initiation and propagation is about 10–20% more extent on the left side. There are more fractures and they are fairly longer compared to fractures at the right borehole boundary. The amount of fracture initiation and propagation is increased by 16% in the section 0.5 m compared to section 1.5 m below tunnel floor.

3.4 Deformation at the pillar boundaries

The displacement of the pillar boundary has been investigated in sections 1.5 m and 0.5 m below the tunnel floor. The notation of angle along the pillars is presented in Figure 3-4 for corresponding locations.

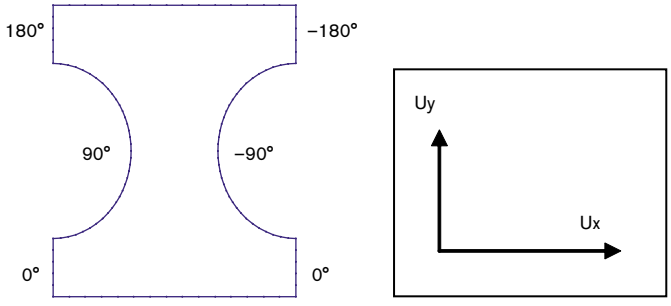

Figure 3-4. *Notation for the location of the pillar boundaries.*

Table 3-2 lists the total displacement at certain points along the pillar from each loading stage. Figure 3-5 and Figure 3-6 show the x- and y-directional displacements along the pillar.

Deformations at all sides are gradually increased according to loading stage. Displacements near central walls are very small compared to areas perpendicular to the tunnel line even though fracturing has occurred.

The confinement of 0.8 MPa mostly affects the deformation of Ux (not Uy), and the deformation is small, less than 2×10^{-5} m.

Since in-situ stress is non-symmetric, displacements at bottom and top of the pillar are slightly different.

There are several reasons for small deformation from modelling at the fractured section /Rinne et al. 2003a/. Actually, it is difficult to predict how fracturing in the vicinity of the pillar boundaries can influence deformation. The displacement after fracturing is a complex process in real situation. A loose detached block may have 1 mm movement, or 100 mm movement, while the mechanical stability of the remaining part of the rock mass is not affected.

The most of deformations presented here are from the elastic response of intact rock. The shearing fractures gives a slight add, but due to high stiffness of new-initiated fractures the slip is very sparse.

Table 3-2. Total displacement at different angles of the pillar boundary for each loading step.

Angle(°) Depth 1.5 m	Total Displacement (m) Location	Excavation	30 days	60 days	90 days	120 days
	Left Pillar Wall					
0	Bottom	1.80E–03	1.96E–03	2.15E–03	2.26E–03	2.35E–03
90	Side	1.68E–04	1.81E–04	2.10E–04	2.31E–04	2.47E–04
180	Top	1.78E–03	1.94E–03	2.10E–03	2.19E–03	2.27E–03
	Right Pillar Wall					
0	Bottom	1.78E–03	1.88E–03	2.05E–03	2.16E–03	2.25E–03
–90	Side	1.52E–04	2.25E–04	2.49E–04	2.55E–04	2.62E–04
–180	Top	1.73E–03	1.81E–03	1.98E–03	2.08E–03	2.16E–03
Depth 0.5 m						
	Left Pillar Wall					
0	Bottom	2.01E–03	2.17E–03	2.35E–03	2.46E–03	2.55E–03
90	Side	1.93E–04	1.98E–04	2.27E–04	2.48E–04	2.63E–04
180	Top	2.03E–03	2.18E–03	2.35E–03	2.44E–03	2.51E–03
	Right Pillar Wall					
0	Bottom	1.98E–03	2.07E–03	2.23E–03	2.33E–03	2.41E–03
–90	Side	1.70E–04	2.31E–04	2.51E–04	2.54E–04	2.59E–04
–180	Top	1.98E–03	2.07E–03	2.23E–03	2.33E–03	2.41E–03

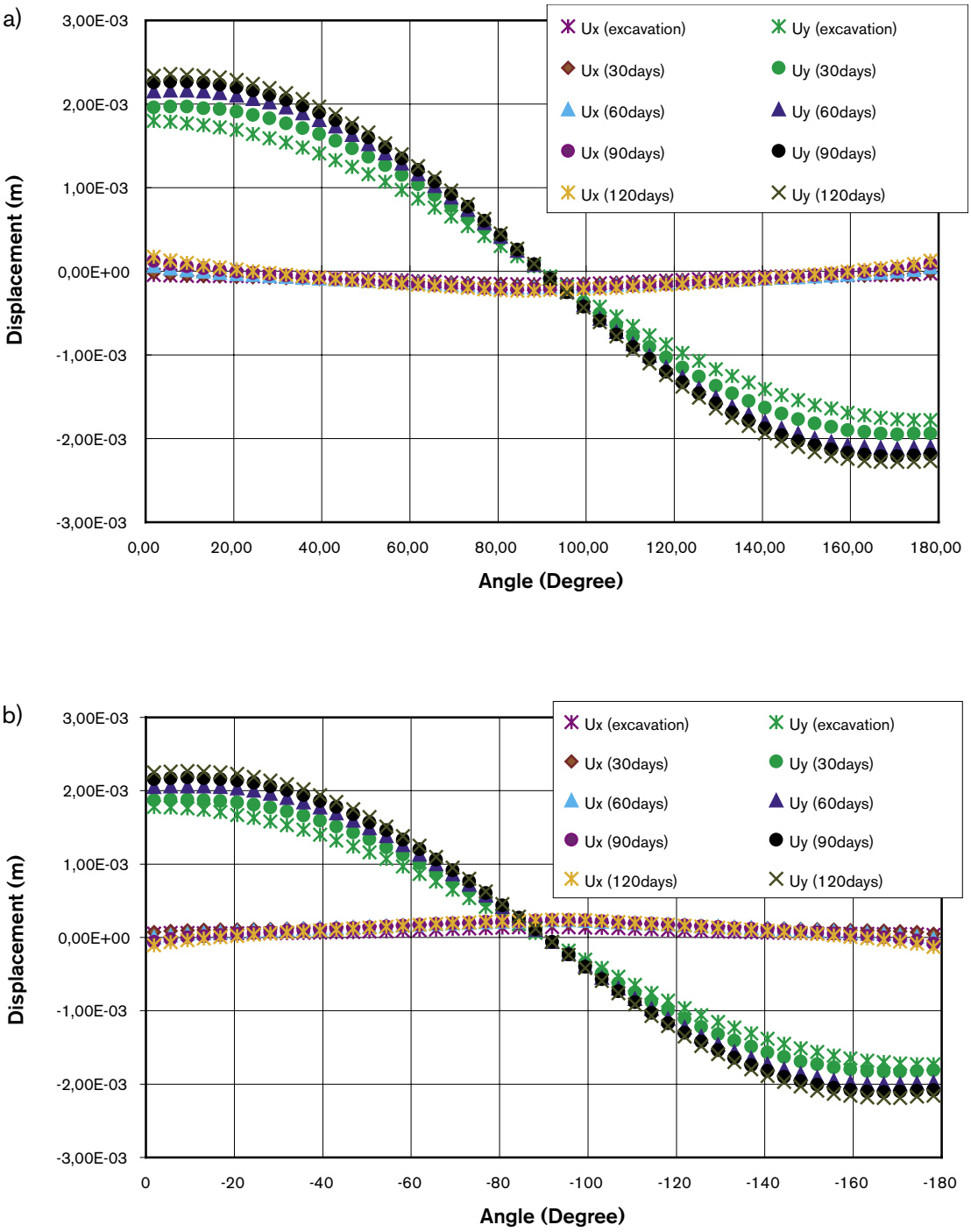

Figure 3-5. *Displacement along pillar boundaries at 1.5 m section below the tunnel floor (Ux: x-displacement, Uy: y-displacement). (a) Left borehole wall. (b) The right (confined) borehole wall.*

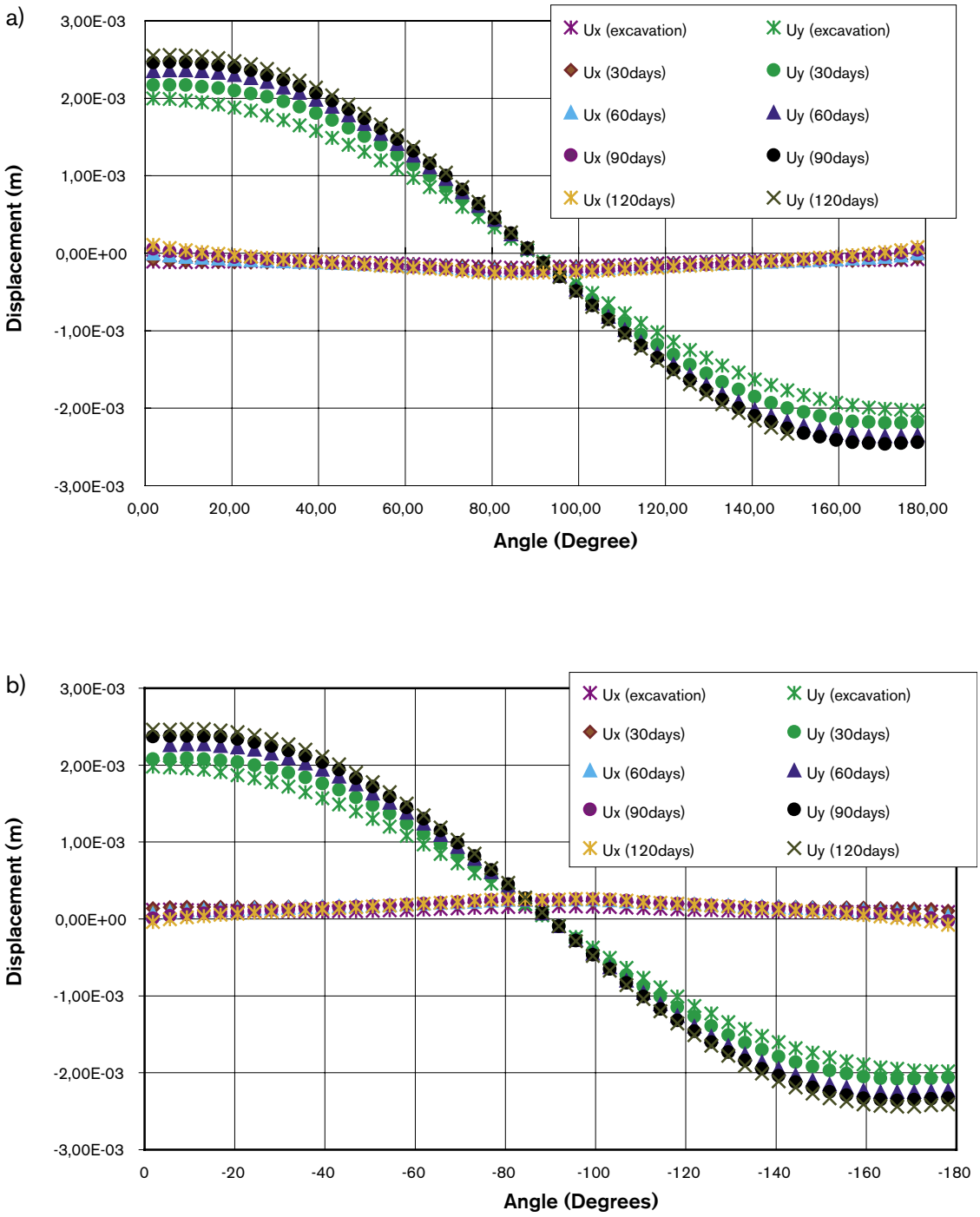

Figure 3-6. *Displacement along pillar boundaries at 0.5 m section below the tunnel floor (Ux: x-displacement, Uy: y-displacement). (a) Left borehole wall. (b) The right (confined) borehole wall.*

3.5 AE evolution

The fracture initiation from intact rock and the AE prediction options are described in /Rinne et al, 2003a, Part II: "Modelling Fracture Initiation and Acoustic Emission (AE) Using FRACOD"/.

Figure 3-7 represents the evolution of AE events during fracturing process for the section 0.5 m below tunnel floor. In the figures, red dots represent the current active AE events. AE events are stepwise modelled and the intensity of AE events is proportional to the degree of fracturing.

The AE events in the section 1.5 m below tunnel floor appears to be very similar to AE's modelled 0.5 m below the floor. Most intense AE events occur at the central pillar wall after excavation due to intense fracture propagation for both sections.

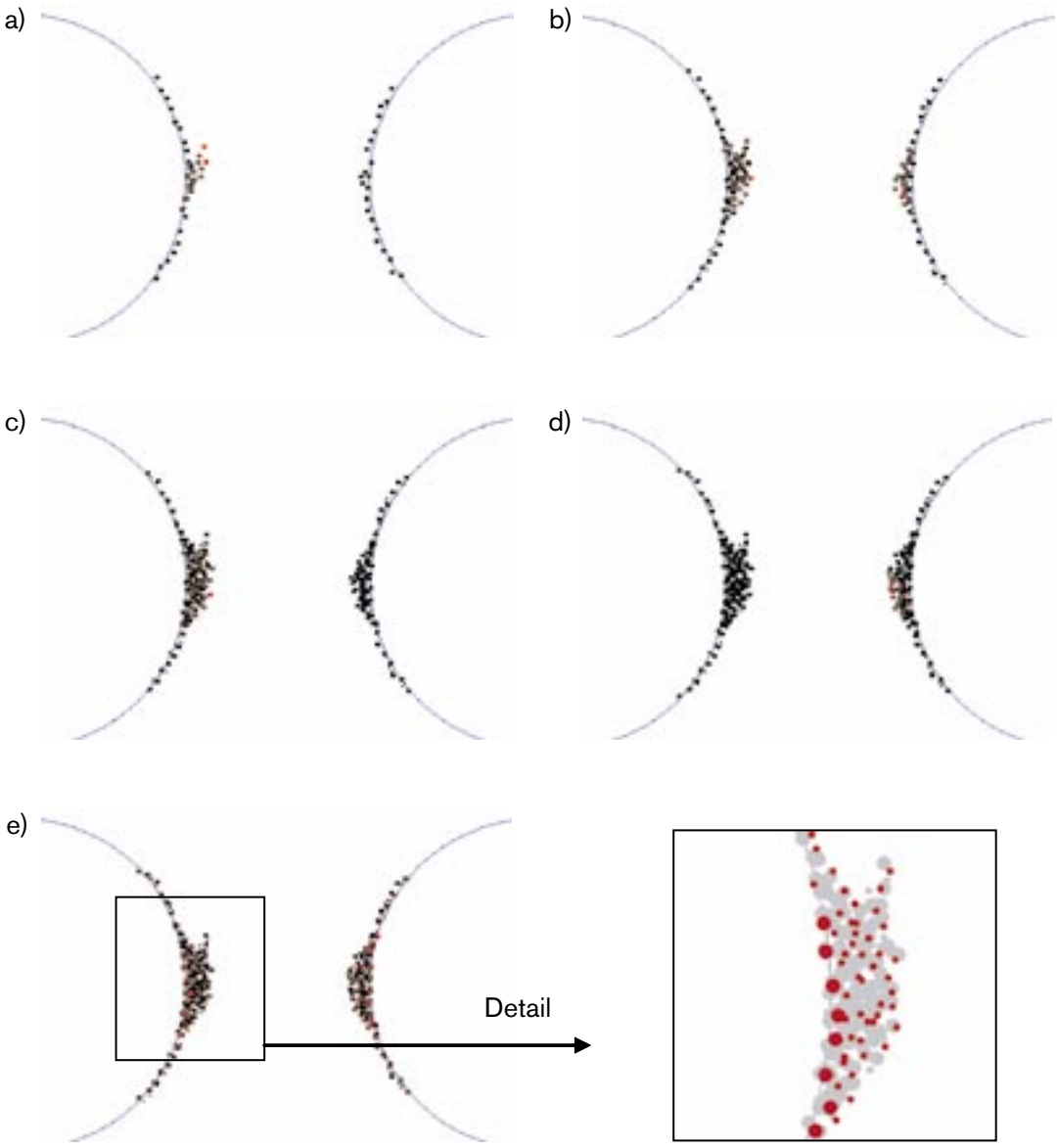

Figure 3-7. *AE evolution in section 0.5 m below the tunnel floor. (a) After excavation. (b) During 30 days of heating. (c) During 60 days of heating. (d) During 90 days of heating. (e) During 120 days of heating. Red dots are current active AE events and the size is proportional to the AE intensity.*

3.6 Summary of the results

Table 3-3 summarizes the result of pillar models together with maximum stress and deformation values.

All models show stable behaviour in terms of both stress and deformation though extensive fracture initiation and propagation have occurred along central pillar walls at both depths below tunnel floor. In all cases, stresses after fracturing are smaller than elastic ones due to stress relaxation. After applying hydraulic pressure, only slight maximum stress change occurred. Critical condition for unstable spalling is not anticipated after 120 days of heating for both 0.5 m and 1.5 m sections. According to the modelling results, the amount of loading should be increased to observe unstable fracturing process in the whole pillar region.

Table 3-3. Summary of results for each loading step.

Loading step		1.5 m	Comments on fracturing	0.5 m	Comments on fracturing
Excavation	M.C*	120	Fracture initiation along pillar walls	134	Fracture initiation along pillar walls and minor propagation at central pillar
	M.T**	3.73		4.29	
	M.D***	1.83		2.06	
30 days	M.C	139	Fracture propagation	154	Fracture propagation and coalescence
	M.T	7.08		6.27	
	M.D	2.00		2.23	
60 days	M.C	153	Fracture propagation and coalescence	168	Fracture propagation and coalescence
	M.T	3.66		4.94	
	M.D	2.21		2.42	
90 days	M.C	160	Fracture propagation	175	Fracture propagation and coalescence
	M.T	3.64		4.75	
	M.D	2.33		2.54	
120 days	M.C	165	Few fracture initiation in the vicinity of the pillar wall and fracture propagation	182	Slight fracture initiation at the right borehole boundary
	M.T	3.62		4.63	
	M.D	2.43		2.64	

* M.C : Maximum compressive stress (MPa).

** M.T: Maximum tensile stress (MPa).

*** M.D: Maximum displacement (×e-3m).

4 Effect of pre-existing fractures

4.1 Fracture properties

Numerical sensitivity analysis of fracture parameters have been carried out using simple loading configurations /Rinne, 1999, 2000/. Most of fracture parameters are highly stress dependent and the effect of a certain fracture parameter depends on the loading configuration.

Preliminary APSE pillar models including possible pre-existing fractures have been investigated by FRACOD /Rinne et al. 2003a/. Calculations suggest that pre-existing fractures can reduce the stress concentration in the critical pillar region because they allow larger deformation compared to intact rock. Fracturing is reduced compared to the intact case due to lower stress level at the borehole wall. However, instability may occur when pre-existing fractures are located inside the pillar in such a way that they cause high stress concentration.

Fracture stiffnesses control strongly the local stress redistribution as well as the deformation in the vicinity of the fracture. A fracture with low stiffness gives large deformation and the fracture response to stresses and deformations like a hole.

Following the earlier modelling study more detailed rock mass characterization has been attained from the experiment tunnel. In the following examples some sensitivity studies with real fracture geometries are presented for the section 0.5 m below tunnel floor. By the time the modelling was completed, no site specific fracture parameters were available for the mapped discontinuities. The following examples should be regarded as guidance for further detailed modelling work.

4.2 Pillar model with discrete fractures

Figure 4-1 presents a preliminary fracture map of discontinuities at location where the boreholes are planned to be drilled by a TBM machine. A simplification for numerical modelling of the pillar area is also presented. The pillar area is cut by a branched shear zone and by several vertical fractures. For the following modelling work some assumptions were made:

1) The material properties in the shear zone (SZ_V and SZ_S) most likely differ from the Äspö diorite. The contact between the shear zone and the diorite is most likely to be very stiff and the cohesion is high.
2) The stiffness of the open structure (Struct_open) is most likely to be low and its cohesion is zero.
3) The NW fracture (NW_struct_1) has been identified as water bearing fracture and its cohesion is supposed to be zero.

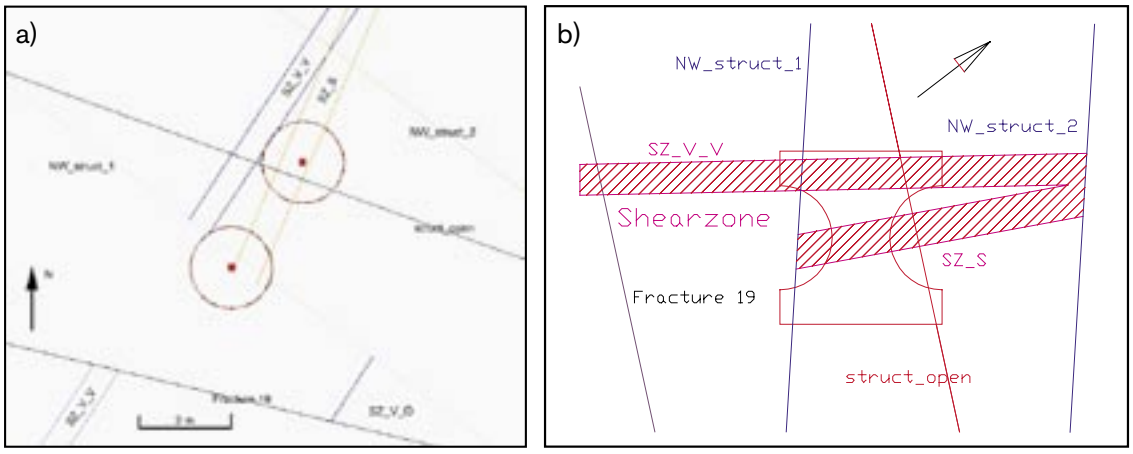

Figure 4-1. *Feactures in section 0.5 m below tunnel floor. (a) Fracture trace map from the test tunnel (Golders). (b) Simplified geometry of fractures and the shear zone crossing the pillar area.*

4.3 AE response from discontinuities

In the first example the fracture initiation was restricted to study the AE response of mapped discontinuities. Stresses referring to 120 days of heating have been applied. The applied fracture parameters are shown in Table 4-1. Other parameters applied are listed in Table 2-1.

Here the aim was not to use the most realistic parameters, rather to demonstrate the capacity to simulate the Acoustic Emission from different kind of discontinuities.

As can be seen on Figure 4-2(a), the most important source of Acoustic Emission is the "Sruct_open" on the right side of the pillar. Both NW_struct_1 and Struct_open will slip after applying excavation induced stresses. The NW_struct_1 produces less seismic activity compared with Struct_open due to higher fracture stiffness. The Shear zone will not give any AE response on loading with applied high stiffness.

It can be noted from Figure 4-2(b) that the stress distribution of s_1 is not remarkably altered while the minor stress distribution is more effected by discontinuities (right up corner in Figure 4-2(c).

Table 4-1. Input parameters for existing discontinuities at APSE.

Discontinuity	Fracture stiffness K_s and K_n	Fracture friction angle	Cohesion	Notes: Dilation angle for all =2.3°
NW_struct_1	26,800 GPa/m 26,800 GPa/m	31°	0 MPa	/Staub et al. 2004/
Struct_open	35.5 GPa/m 61.5 GPa/m	31°	0 MPa	/Staub et al. 2003/
Contact of the shear zone and Äspö diorite	Stiff contact.	49°	31 MPa	Appendix 1. Only fracture sliding may cause shear deformation.

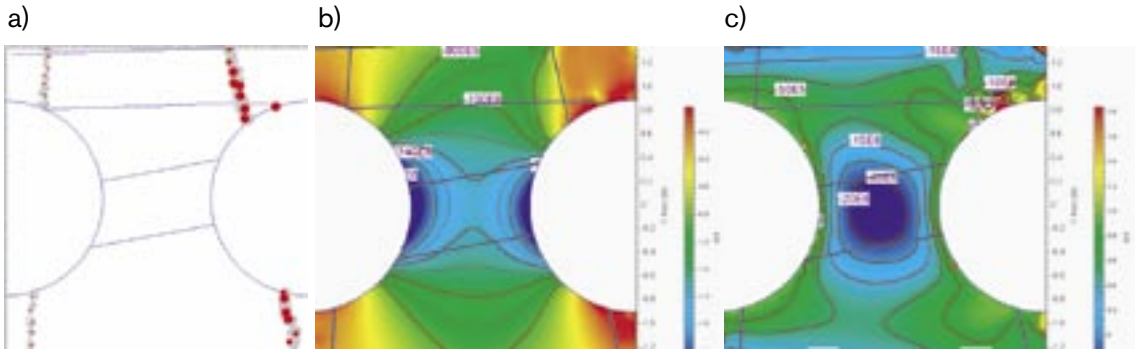

Figure 4-2. *Simulation of section 0.5 m below tunnel floor after applying stresses from 120 days heating. (a) Modelled AE from the pre-existing fractures (b) σ_1 distribution. (c) σ_3 distribution.*

4.4 Fractures NW_struct_1 and Struct_open

In the following example the effect of fractures NW_struct_1 and Struct_open was investigated. The Shear zone was removed by considering it to have the same material properties as Äspö diorite and stiff contacts, as modelled in the previous example. Results presented in Figure 4-3 suggests that the NW_struct_1 and Struct_open do not change remarkably the failure pattern in the mid pillar (when Shear zone is ignored).

4.5 Shear zone

In this example a low stiffness of the shear zone contact has been applied to study the effect of larger deformations from discontinuities in the critical pillar section. In the first trial the same stiffness was applied as for the Struct_open K_n/K_s =(35.5 GPa/m) / (61.5 GPa/m). Calculations appeared to be unstable, producing large deformations and unrealistic high tensile stresses. Applied K_n is valid with normal stress of 23 MPa and for K_s in the range of 2 MPa–6 MPa of normal stress /Staub et al. 2003/. They seem to be too low to be applied in a highly stressed area like in the stressed pillar.

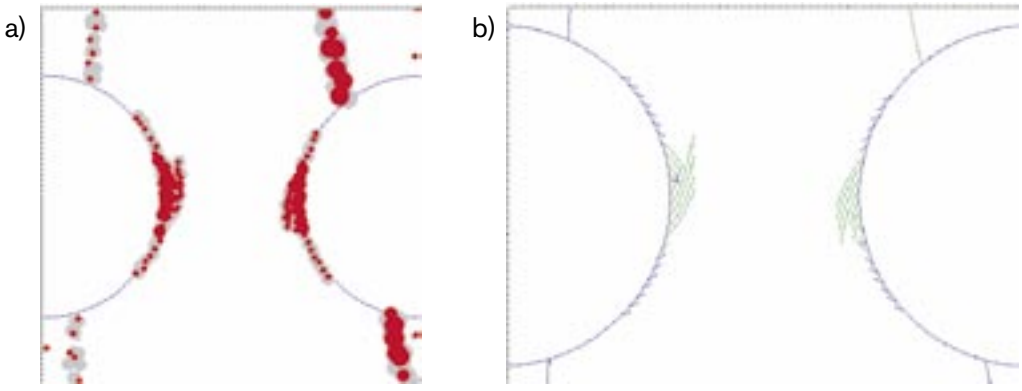

Figure 4-3. *The effect of pre-existing discontinuities on failure. (a) Modelled AE's after applying stresses from 120 days heating. (b) Fracture pattern (compare with Figure 3-3e).*

For natural joints, the ratio $k=K_n/K_s$ = (61.5 GPa/m) / (35.5 GPa/m) =1.7, seems also to be exceptionally low. As a general rule K_n/K_s is seldom less than 10 and may be even 100 /Barton, 2003/.

After 120 days of heating the average compressive stress in the pillar is >100 MPa, and the normal stiffness is expected to be much higher than 61.5 GPa/m. Considering that normal stiffness is at least 10 times the shear stiffness, we get more realistic values for natural fractures under highly compressed loading. Applying K_n/K_s=(355.0 GPa/m) / (35.5 GPa/m) for the Shear zone contact we get the failure pattern as presented in Figure 4-4.

This example suggests that yielding discontinuities intersecting the pillar decrease the amount of failure. The area of maximum compressive stresses is reallocated and the asymmetry of stresses is increased. New distribution of stresses is more apparent for σ_3 compared to σ_1. Note the strong redistribution of σ_3 close to the boundaries of the shear zone (Figure 4-4d).

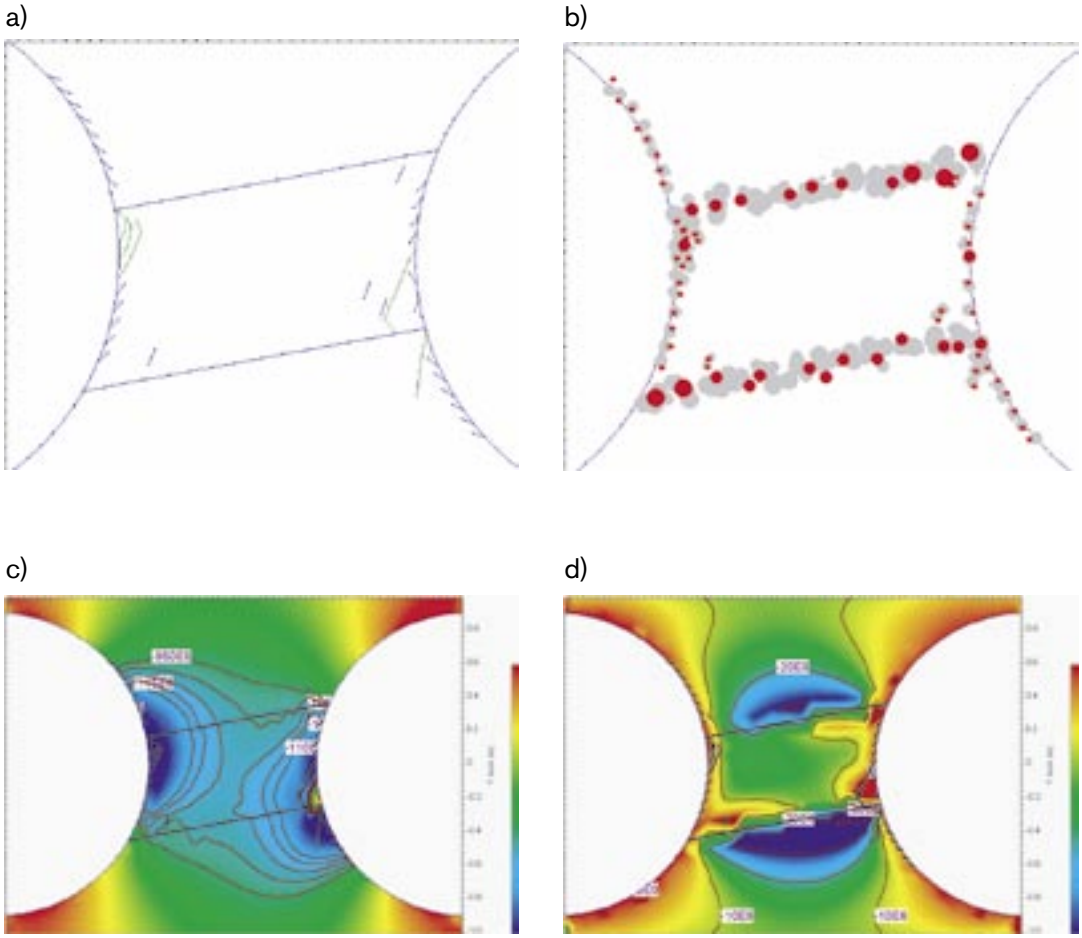

Figure 4-4. *Modelling of section 0.5 m below tunnel floor after applying stresses from 120 days heating. (a) Fracture pattern affected by the Shear zone. (b) Modelled AE (c) σ_1 distribution. (c) σ_3 distribution.*

5 Model accuracy

The element size defines the model accuracy; the more elements the more accurate are the results. However, increase of number of elements increases the calculation time exponentially and enhances the risk of numerical problems and unstable calculations. Element size is a compromise between accuracy and calculation capacity.

The number of elements must be sufficient when studying in detail behaviour of fractures close to either an excavation boundary or another fracture. In the region where stress variation is not significant, the effect of the element size is less apparent.

The effect of element size and accuracy of FRACOD have been studied by /Rinne, 1999, 2000/. Accuracy of FRACOD calculations have also been compared with theory of classical hydraulic fracturing /Lee et al. 2003/. The theoretical breakdown pressure for fracture initiation and FRACOD simulations agreed well (error <2%) considering a limited number of elements (32 elements) in the simulated borehole.

The current version of the code can handle a model consisting of about 400 elements. About 100 to 120 elements at the start is the upper limit for calculation on a standard PC. The APSE pillar model without pre-existing fractures has 100 elements. After 120 days of heating the initiated and extended fractures doubles the model size.

The element size defining the model boundary decides the length of a new fracture. In "APSE Pillar model" the element size is about 10 cm. A sensitivity analyse was conducted for APSE model with varying element size. The results are generally consistent, although the fracture pattern may be affected, particularly for models with large elements.

The accuracy of the reconstructed stress model has been presented in Appendix 2 and more detailed in /Rinne et al. 2003a/.

Uncertainties in APSE prediction has been discussed in /Rinne et al. 2003a/.

6 Conclusions

The FRACOD code has been updated with many new features and they have been successfully applied to model different loading stages of Äspö pillar experiment. The following conclusions are based on results from numerical predictions by the updated code and updated field data. The predictions are made for isotropic and homogenous Äspö diorite.

6.1 Pillar response on planned loading sequences

Calculations suggest that the planned loading geometry will induce stresses that are close to the limit for fracture initiation with given material properties. Minor fracture initiation may take place in the vicinity of the boreholes before heating.

Heating induces minor spalling at central pillar wall for both 0.5 m and 1.5 m sections below the tunnel floor, but the area of spalling is found to be limited.

The core of the pillar remains intact for stress conditions corresponding to 120 days of heating.

Confining pressure of 0.8 MPa in one of the borehole slightly decrease the maximum stresses at the borehole wall. Calculation results suggest that the stabilizing effect is limited.

Small disturbances in the stress field, for example caused by unsymmetrical heat flow, or pre-existing discontinuities might affect the fracture pattern. In some models one or several fractures extend outside the area of spalling. However, these fractures were not found to propagate in to the centre part of the pillar in unstable manner.

6.2 Pre-existing fractures

Calculations results suggest that borehole crossing pre-existing fractures will reduce the stress concentration in the critical pillar region because they allow larger deformation compared to intact rock. Fracturing is reduced compared to the intact case due to decreased stress at the borehole wall.

Short, barren, pre-existing fractures may disturb the stress distribution and may locally cause extensive fracture initiation and propagation near the fracture tip. The effect depends on location, size, orientation and properties of the fracture.

6.3 Sensitivity analyses of fracture parameters

A sensitivity analysis was made to investigate the effect of new input data on failure models. The sensitivity analysis suggest that updated parameters and stress data increase slightly the area of failure compared to the previous model reported in /Rinne et al. 2003a/.

The impact is not significant and the middle part of the pillar remains stable after applying stresses from excavation and thermal load of 120 days.

Fracture properties, for both pre-existing and new fractures, have a strong effect on the fracturing process. Beside cohesion and friction angle, the fracture stiffness and fracture toughness are important parameters controlling the failure. Many uncertainties still exist about these properties, especially for new initiated fractures under high loading conditions. Due to the many variables of the model at this stage, a comprehensive sensitivity analyse of new fractures was not made. More in depth analyse of the combined effect of applied parameters are suggested. Especially the ratio between K_n/K_s should be studied more carefully.

6.4 Model improvement

A number of uncertainties and limitations in describing the deformation in the fractured zones exist. FRACOD apply constant values for fracture toughness and fracture stiffness, although these parameters are highly stress dependent. Barton-Bandis joint model would directly simulate the joint behaviour. For model improvement, we suggest implementing the BB model in FRACOD to simulate joint behaviour more realistically.

The effect of different joints and fractures recently mapped in the experiment area should be analyzed more in detail. The material properties of the shear zone cutting the pillar should be investigated and considered in stress and failure models. Acoustic Emission monitoring results might help to estimate the fracture properties of existing discontinuities.

A shortage of the Boundary Element method is its ability to simulate different materials in one and the same model. FRACOD has recently been updated for analysis for multi-region problems. It simulates several material domains in the same model using the mechanical and fracture mechanics properties of each region. The new improvement is suggested to be used for the shear zone model, when appropriate data of the shear zone is available.

7 Predictions

SKB assigned the task to make specific spalling predictions by giving the four questions listed below:

1. What is the failure criterion, i.e. where does one obtain spalling?
2. What tangential stress is required to initiate spalling?
3. How deep will the spalling propagate as a function of stress, i.e. depth of failure?
4. What is the effect of confining stress on 1, 2 and 3 above?

This section is the FRACOD interpretation to these questions.

7.1 What is the failure criterion for spalling, i.e. where does one obtain it?

In FRACOD the spalling is simulated by three processes; fracture initiation, failure of potential fracture planes and by fracture propagation. The criteria used in FRACOD to detect fracture initiation has been described thoroughly in /Rinne et al. 2003a, Part II, section 2.3/. Fracture initiation often starts from microcrack formation at a stress level of 0.3–0.6 of the rock strength. In this study we assume that when the stress reaches 50% of the rock strength at a given location, a potential macrocrack or a failure plane may form. This discontinuity, however, has the intact rock strength. Local failure may take place and the fracture may propagate only when the strength of this surface is exceeded during the subsequent increase in stress. For this reason the level for fracture initiation is not critical for the final failure.

Tensile strength criterion is used in the direction perpendicular to the tensile stress. For shear fracture initiation, the Mohr-Coulomb failure criterion is used. Fracture initiation at boundaries of the boreholes as well as from the intact rock is considered.

Fracture propagation is modelled by the F-criterion described comprehensively in /Shen and Stephansson, 1994/. According to the F-criterion, in an arbitrary direction (θ) at a fracture tip there exists a F-value, which is calculated by

$$F(\theta) = \frac{G_I(\theta)}{G_{Ic}} + \frac{G_{II}(\theta)}{G_{IIc}}$$

where G_{Ic} and G_{IIc} are the critical strain energy release rates for mode I and mode II fracture propagation; $G_I(\theta)$ and $G_{II}(\theta)$ are strain energy release rates due to the potential mode I and mode II fracture growth of a unit length. The direction of fracture propagation will be the direction where F reaches the maximum value. If the maximum F reaches 1.0, fracture propagation will occur.

7.2 What is the tangential stress required to initiate spalling?

Theoretically, applied parameters (cohesion c=31 MPa and intact rock friction φ=49° angle) gives a uni-axial strength of 166 MPa. FRACOD calculations suggest fracture initiation to start from the borehole boundary in the narrowest section of the pillar, when the tangential stresses reach a value of about 80 MPa /Rinne et al. 2003a, Part I, Figure 4-3/. Following the stress increase, the initiation will progress along the borehole wall.

FRACOD APSE models suggest fracture failure and fracture propagation when the maximum tangential stress exceeds 130 MPa. There are two reasons why the slippage (failure) of new fractures takes place before 166 MPa, as suggested by Mohr-Coulomb criterion. If the fracture stiffness of a new fracture is very high, the code would not feel its existence. If the stiffness is not that high, as in our case, there will be an additional deformation so the new fracture is felt as a defect. The stress redistributes around it and cause lower normal stress and higher shear stress. In addition, if there is more than one new fracture generated at once, the fractures affect each other and may result in early fracture slippage.

7.3 How deep will spalling propagate as a function of stress, i.e. depth of failure.

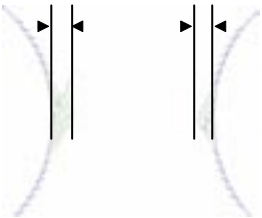

Figure 7-1. *Depth of spalling is defined perpendicular from the tangent of the narrowest section of the pillar (horizontal section). Results are presented in Table 7-1.*

Table 7-1. Depth of spalling as a function of stresses for each loading step.

Section	Excavation	30 days	60 days	90 days	120 days
Section 1.5 m below tunnel floor					
Maximum compressive stress (elastic model)	122.5 MPa	145.3 MPa	161.7 MPa	169.5 MPa	175.8 MPa
Left borehole boundary	Only fracture initiation	0.11 m	0.13 m	0,13 m	0.13 m
Right borehole boundary	Only fracture initiation	0.10 m	0,12 m	0.12 m	0.12 m
Section 0.5 m below tunnel floor					
Maximum compressive stress (elastic model)	140.2 MPa	162.8 MPa	179.3 MPa	187.1 MPa	193.4 MPa
Left borehole boundary	0.11 m	0.13 m	0.13 m	0,15 m	0,15 m
Right borehole boundary	0.04 m	0.10 m	0.12 m	0.13 m	0,13 m

7.4 The effect of confining stress on 1, 2 and 3

The confining stress for fracture initiation is taken into account in the Mohr-Coulomb failure criterion. The confinement for fracture propagation is considered by calculating the critical strain energy release rate for both mode I and mode II failure in varying directions.

The maximum compressive stress decrease and the confinement increases from the borehole boundary toward the pillar central. Level of confinement where the fracture propagation starts is less than $\sigma_3 < 5$ MPa and the fractures will not propagate inside the region where confinement is higher than $\sigma_3 > 20$ MPa (see Figure 3-2).

The modelled effect of confining pressure from hydraulic pressurization has been presented in chapter 3.3.

8 References

Andersson J C, 2003. Äspö Hard Rock Laboratory. Äspö Pillar Stability Experiment. Feasibility Study. SKB IPR-03-01, Svensk Kärnbränslehantering AB.

Andersson J C, Rinne M, Staub I, Wanne T, 2003. The ongoing Äspö pillar stability experiment. GeoProc2003 Conference. 13–15.10.2003 KTH, Stockholm. Elsevier Science (in press).

Backers T, 2003. Determination of Mode I and Mode II Fracture Toughness and Fracture Normal Stiffness of Äspödiorite. Technical Report GFZ Potsdam, September 2003 (in Staub et al. 2004).

Bandis S C, Lumsden A C, Barton N R, 1983. Fundamentals of rock joint deformation. Int. J. Rock Mech. Sci. & Geomech. Abstr. 20:249–268.

Barton N R, 1986. Deformation phenomena in jointed rock. Geotechnique. 36:147–167.

Barton N, 2003. Äspö Hard Rock Laboratory. Äspö Pillar Stability Experiment. Q-logging of the APSE Tunnel at Äspö. For rock quality assessment and for development of preliminary model parameters. SKB IPR-04-07, Svensk Kärnbränslehantering AB.

Fredriksson A, Staub I, Janson T, 2003. Äspö Hard Rock Laboratory. Äspö Pillar Stability Experiment. Design of heaters and preliminary results from coupled 2D thermo-mechanical modelling. SKB IPR-03-03, Svensk Kärnbränslehantering AB.

Klee G, Rummel F, Weber U, 2001. Äspö Hard Rock Laboratory. Rock stress measurements in Oskarshamn. Hydraulic fracturing and core testing in borehole KOV01. SKB IPR-02-01, Svensk Kärnbränslehantering AB.

Kuula H, 2003. UCS and tri-ax and Brazil tests from KQ0064G01&07. Preliminary test report. HUT, Rock Engineering, Helsinki (in Staub et al. 2004).

Lee H S, Jing L, 2003. An inverse stress reconstruction algorithm for modelling coupled thermo-mechanical effects of rock structures, Accepted for publication in Engineering Analysis with Boundary Elements.

Lee H S, Shen B, Stephansson O, Rinne M, 2003. Modelling of COUPLE hydraulic fracturing experiment with FRACOD. Fracom Ltd. Unpublished report for Kyoto University and Hazama Corporation, Japan.

Nordlund S, Li C, Carlsson B, 1999. Äspö Hard Rock laboratory. Prototype repository. Mechanical properties of the diorite in the prototype repository at Äspö HRL. Laboratory tests. SKB IPR-99-25, Svensk Kärnbränslehantering AB.

Rinne M, 1999. BEMF-Code Testing. Mixed mode fracture propagation in the vicinity of a circular opening in crystalline bedrock. Draft report 99-12-06, Svensk Kärnbränslehantering AB.

Rinne M, 2000. Propagation of rock fractures in the vicinity of a canister hole for spent nuclear fuel. Licentiate Thesis. Royal Institute of Technology, Engineering Geology. Stockholm, Sweden.

Rinne M, Shen B, Lee H S, 2003a. Äspö Hard Rock Laboratory. Äspö pillar stability experiment. Part I: Modelling of fracture stability by FRACOD. Part II: Modelling Fracture Initiation and Acoustic Emission. Part III: Reconstruction of Stress Field Using an Inverse Technique. SKB IPR-03-05, Svensk Kärnbränslehantering AB.

Rinne M, Shen B, Lee H S, Jing L, 2003b. Thermo-mechanical simulations of pillar spalling in SKB APSE test by FRACOD. GeoProc2003 Conference. 13–15.10.2003 KTH, Stockholm. Elsevier Science (in press).

Shen B, Stephansson O, 1994. Modification of the G-criterion of crack propagation in compression. Int. J. of Engineering Fracture Mechanics. 47(2), 177–189.

Shen B, 2002. FRACOD Version 1.1, User's manual. Fracom Ltd.

Staub I, Janson T, Fredriksson A, 2003. Äspö Pillar Stability Experiment, Geology and properties of the rock in TASQ. SKB IPR-03-02, Svensk Kärnbränslehantering AB.

Staub I, Andersson J C, Magnor B, 2004. Äspö Pillar Stability Experiment, Geology and mechanical properties of the rock in TASQ. SKB R-04-01, Svensk Kärnbränslehantering AB.

Wanne T, Johansson E, Potyondy D, 2004. Äspö Pillar Stability Experiment, Final Coupled 3D thermo – mechanical modeling. Preliminary Particle – mechanical modeling. SKB R-04-03, Svensk Kärnbränslehantering AB.

APSE publications

Andersson, J. Christer
Äspö Pillar Stability Experiment, Summary of preparatory work and predictive modelling. SKB R-03-02, Svensk Kärnbränslehantering AB.

Andersson, J. Christer and Martin, C.D. and Christiansson, R.
SKB's Äspö Pillar Stability Experiment, Sweden.
In the proceedings of Gulf Rocks 2004, the 6th North American Rock Mechanics Symposium (NARMS), Houston, Texas, June 5–9, 2004.

Andersson, J. Christer and Rinne, M. and Staub, I. and Wanne, T.
Stephansson, O. and Hudson, J.A. and Jing, L. (ed.)
The on-going pillar stability experiment at the Äspö Hard Rock Laboratory, Sweden.
In the proceedings of GeoProc 2003, International conference on coupled T-H-M-C processes in Geo-systems: Fundamentals, Modelling, Experiments & Applications. KTH, October 13–15, 2003, Stockholm, Sweden, p. 385–390

Andersson, J. Christer and Martin, C.D.
Katsuhiko Sugawara and Yuozo Obara and Akira Sato (ed.)
Stress variability and the design of the Äspö Pillar Stability Experiment. In the proceedings of the third international symposium on rock stress. RS Kumamoto '03, 4–6 November 2003, Kumamoto Japan, p. 321–326

Fredriksson, Anders and Staub, I. and Outters, N.
Äspö Pillar Stability Experiment, Final 2D coupled thermo-mechanical modelling. SKB R-04-02, Svensk Kärnbränslehantering AB.

Rinne, Mikael and Lee, H-S. and Shen, B.
Äspö Pillar Stability Experiment, Modelling of fracture development of APSE by FRACOD. SKB R-04-04, Svensk Kärnbränslehantering AB.

Staub, Isabelle and J.C. Andersson and B. Magnor
Äspö Pillar Stability Experiment, Geology and mechanical properties of the rock in TASQ. SKB R-04-01, Svensk Kärnbränslehantering AB.

Wanne, Toivo and Johansson, E. and Potyondy, D.
Äspö Pillar Stability Experiment, Final Coupled 3D thermo – mechanical modeling. Preliminary Particle – mechanical modeling. SKB R-04-03, Svensk Kärnbränslehantering AB.

Appendix 1

Modelling of fracture development of APSE by FRACOD

Parameter Sensitivity Analyses

Mikael Rinne, Baotang Shen, Hee-Suk Lee
Fracom Ltd

March 2004

Contents

A1 Parameter sensitivity analyses

A1.1 Introduction

A sensitivity analysis on FRACOD parameters was made to investigate the effect of new input data on failure models. Each parameter was tested separately, while others were kept constant (Table A1-1). Same pillar model geometry and loading stresses were used as in the previous modelling phase /Rinne et al. 2003a/. Stress condition in the section 0.5 m below tunnel floor has been considered. Due to long calculation time, loading up to 30 days of heating induced stresses instead of 120 days has been applied.

Here the described section is named Standard Case, Figure A1-1 and Table A1-1.

Table A1-1. Input data in the Standard Case, analysed and suggested new parameters.

Parameter	Value and unit (applied in the previous study)	Analysed	Suggested new value
Intact rock			
Young's modulus:	68 GPa		55 GPa (x)
Poisson's ratio:	0.24		0.26 (x)
Cohesion:	31 MPa	X	
Friction angle:	49°	X	
Tensile strength	14.8 MPa	X	14.3 MPa

Parameter	Value and unit (applied in the previous study)	Analysed	Suggested new value
Fractures			
Fracture toughness in mode I	2.54 MPa $m^{1/2}$	X	3.80 MPa $m^{1/2}$
Fracture toughness in mode II	6.35 MPa $m^{1/2}$	X	
Normal stiffness, K_n for pre-existing (old) fractures	615 GPa/m		See main report
Shear stiffness, K_s for pre-existing (old) fractures	35.5 GPa/m		See main report
Fracture friction angle	31°		
Cohesion of pre-exiting fractures	1 MPa		
Properties of newly created fresh fractures			
K_n Shear fractures	4,643 (GPa/m)	X	26,976 (GPa/m)
K_s Shear fractures	Shear restricted	X	26,976 (GPa/m)
Friction angle	49.0 (°)	X	
Cohesion	31 (MPa), 0 after sliding	X	
Dilation angle	2.3 (°)		
K_s Tensile fractures	Shear restricted	X	26,976 (GPa/m)
K_n Tensile fractures	320 (GPa/m)	X	26,976 (GPa/m)
Friction angle	49.0 (°)	X	
Cohesion	31 (MPa), 0 after sliding	X	
Dilation angle	12.1 (°)		

(*) Applied only in the final model with new stress data.

Table A1-2. SKB Suggested input data for APSE modelling (9/10 2003).

Parameter	Value	Unit
Uniaxial Compressive Strength low	130	MPa
Uniaxial Compressive Strength high	210	MPa
Young's modulus, intact rock	75.6	GPa, std. 6.5 GPa
Young's modulus, rock mass	55	GPa
Poisson's ratio, intact rock	0.25	–
Poisson's ratio, rock mass	0.26	–
Friction angle, intact rock	49	Degrees
Friction angle, rock mass	41	Degrees
Cohesion, intact rock	31	MPa
Cohesion, rock mass	16.4	MPa
Tensile strength	14.3	MPa
Normal stiffness, sub. vert. fractures	61.5	GPa/m
Normal stiffness, sub. hor. fractures	21.9	GPa/m
Shear stiffness, sub. vert. fractures	35.5	GPa/m
Shear stiffness, sub. hor. fractures	15.7	GPa/m
Residual angle, sub. vert. fractures	31	Degrees
Residual angle, sub. hor. fractures	30	Degrees
Mode I fracture tiughness, K_{IC}	3.80 ± 0.1	$MPa/m^{1/2}$
Mode II fracture tiughness K_{IIC}	4.4 to 13.5	$MPa/m^{1/2}$
Initial normal stiffness K_{nI}	175 ± 68	GPa/m
High load normal stiffness K_{nH}	26,976 ± 22,757	GPa/m

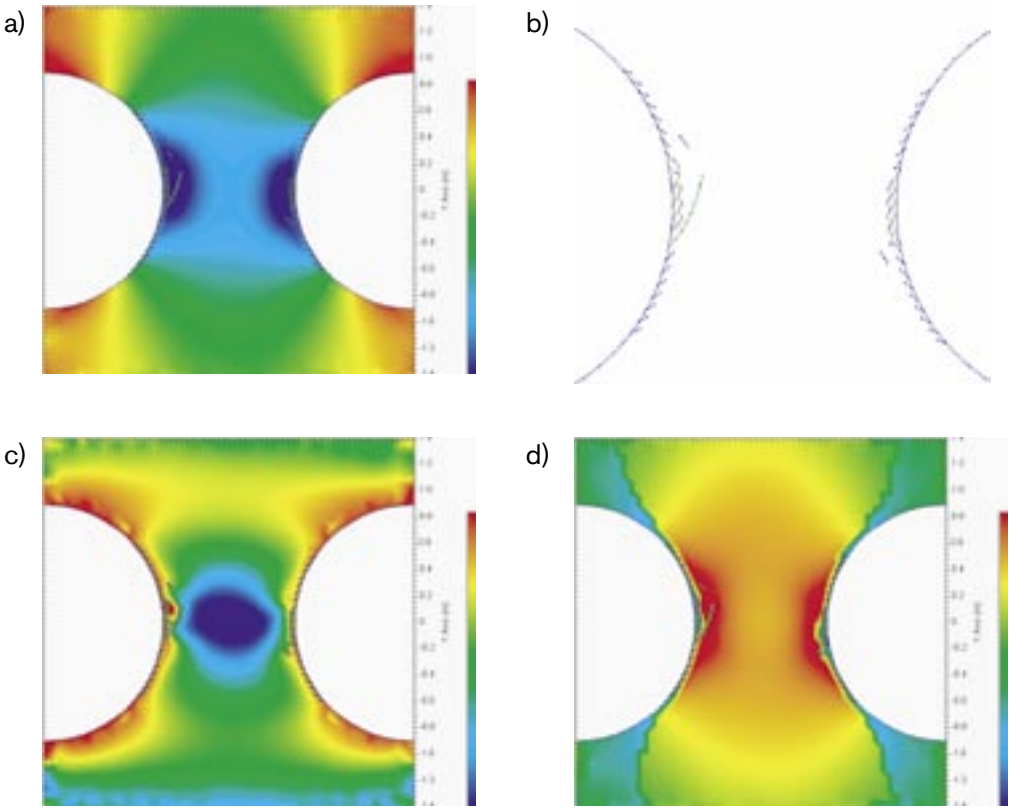

Figure A1-1. *Standard Case. Stress condition in the section 0.5 m below tunnel floor after 30 days of heating. (a) σ_1 distribution, blue area σ_1>140 MPa. (b) Failure pattern. (c) σ_3 distribution, blue area, σ_3>30 MPa. (d) Shear stresses distribution, red area, $\tau \geq 80$ MPa).*

A1.2 Elastic properties

Sensitivity of elastic properties cannot be tested directly by the pillar model because the original stress distribution is determined by boundary displacements. Young's modulus (68 GPa) and Poisson's ratio (0.24) are fixed with the reconstructed stresses and altering elastic properties would distort the stress distribution.

A1.3 Strength parameters of rock and new initiated fractures

A1.3.1 Friction angle and cohesion

Rock strength parameters in FRACOD include internal friction angle (φ), cohesion (c) and tensile strength (σ_t) and the Mohr-Coulomb strength criterion is used.

The new fractures are often curved or kinked. It is assumed that it is unlikely they will experience large shear displacement during fracture propagation in a limited region. Therefore, it is considered that the peak fracture strength (rather than the residual strength) applies to these fractures. Accordingly, it is assumed in FRACOD that the newly created fractures have the same friction angle and cohesion as the intact rock. Once sliding, the fracture will lose its cohesion but the friction angle keeps the same.

Note that the intact rock cohesion was initially used to simulate the case that only limited micro-fractures have been created at lower stress along the potential shear plane but the micro-fractures have not yet formed distinct shear fractures of the minimum length considered in the model (one element length).

Table A1-3. Pillar stability with varying combinations of cohesion and friction angle.

Parameter	Value change	Effect compared to the Standard Case. Fracture Initiation (FI), Fracture propagation (FP).
Cohesion	31=>16.4 MPa	Unstable FI and FP during excavation leads to pillar failure.
Friction angle	49°=>41°	(Refers to Uniaxial Compressive strength of 72 MPa).
Cohesion	31=>24 MPa	Very much FP on both sides of the pillar. Unstable FP during 30 days of heating. (UCS 130 MPa).
Friction angle	(φ=49)°	
Friction angle	49°=>39°	Intense FI and FP. Unstable FP already during excavation. FI in centre part of the pillar. (UCS 130 MPa).
Cohesion	(c =31 MPa)	
Cohesion	31=>39 MPa	Slightly reduced FI during excavation. Slightly increased FP of few fractures after 30 days of heating. (UCS 210 MPa).
Friction angle	(φ=49°)	
Cohesion	49°=>73°	No FI even if 120 days heating load applied. (UCS 210 MPa).
Friction angle	(c=31 MPa)	

SKB suggested rock parameters for updated APSE pillar model are listed in Table A1-2. Property of the modelled rock volume may be found between the rock mass strength and the intact rock strength. Intact rock friction angle (φ =49°) and intact rock cohesion (c=31 MPa) was used in the previous phase models. These values refer to a Uniaxial Compressive Strength (UCS) of 166 MPa according to Mohr-Coloumb failure criterion. The rock mass strength parameters (c=16.4 MPa) and (φ=41°) in Table A1-2 refers to UCS of 72 MPa.

It was suggested that a sensitivity analysis with Low UCS (130 MPa) and with High UCS (210 MPa) should also be made. In Table A1-3 the sensitivity analysis is presented for various combinations of the friction angle (Φ) and cohesion (c).

Calculations suggest that for the pillar model, low values of c and φ lead to unstable fracture propagation already during the excavation phase. The highest modelled friction angle (73°) prevents fracture initiation and the pillar response is elastic. As expected, cohesion and friction angle are sensitive parameters controlling strongly the pillar failure.

A1.3.2 Tensile strength

Calculations were made by reduced tensile strength from 14.8 to 14.3 MPa. The max tensile stress in the model will not exceed 14.3 MPa. Slight reduction of tensile strength has no effect on failure pattern in the actual loading configuration.

A1.4 Fracture toughness mode I

Mode I Fracture toughness (K_{IC}) of rocks near Äspö area has been determined by /Klee et al. 2001/. According to these tests the fracture toughness of 2.54 MPa $m^{1/2}$ was used in the previous modelling phase. Following the previous study the Mode I fracture toughness has been determined on Äspö diorite samples from borehole KA3376B01 /Backers, 2003/. The average value of Mode I fracture toughness is 3.8 ± 0.1 MPa $m^{1/2}$.

Increase of Mode I Fracture toughness (K_{IC} 2.54 to 3.80 MPa $m^{1/2}$) will slightly increase the fracture propagation in the pillar model. However, the effect on the overall failure pattern is minor.

A1.5 Fracture toughness mode II

During the previous modelling work there was no laboratory data available for shear fracture toughness (Mode II) of Äspö rocks, and a best estimate of 6.35 (MPa $m^{1/2}$) was applied. During the spring 2003, Mode II fracture toughness under influence of confining pressure on Äspö diorite samples from borehole KA3376B01 was determined. According to the tests /Backers, 2003/, the Mode II fracture toughness increases from 4.4 to 13.0 MPa $m^{1/2}$ with increase of confining pressure. K_{IIC} becomes almost constant above a confining pressure of about 35 MPa. The confinement in the pillar varies between 0 MPa (borehole boundary) to max 35 MPa (inner section of the pillar).

Mode II fracture toughness (K_{IIC}) seems not to be very sensitive for the result of pillar model above a level of 4.8 MPa $m^{1/2}$. The earlier estimated value 6.35 MPa $m^{1/2}$ corresponds to confining level of ~4 MPa. Because FRACOD only apply constant K_{IIC}, 6.35 MPa $m^{1/2}$ is somewhat conservative, but is a sound average to be used in the pillar model.

Table A1-4. Effect of fracture toughness, Mode II.

Parameter Fracture toughness Mode II (MPa $m^{1/2}$)	Value change	Effect compared to the Standard Case. Fracture Initiation (FI), Fracture propagation (FP).
K_{IIC}, zero confinement	6.35=> 4.40	Standard FI, but strongly increased FP of some fractures (see Figure A1-2.). Due to confinement in the pillar, the constant value 4.4 is valid only in the vicinity of the borehole boundary- and the model overestimates fracture propagation.
K_{IIC}, low confinement	6.35=> 4.80	Very slight difference compared with standard case; K_{IIC}=6.35.
K_{IIC}, high confinement	6.35=> 13.0	Slightly reduced FP.

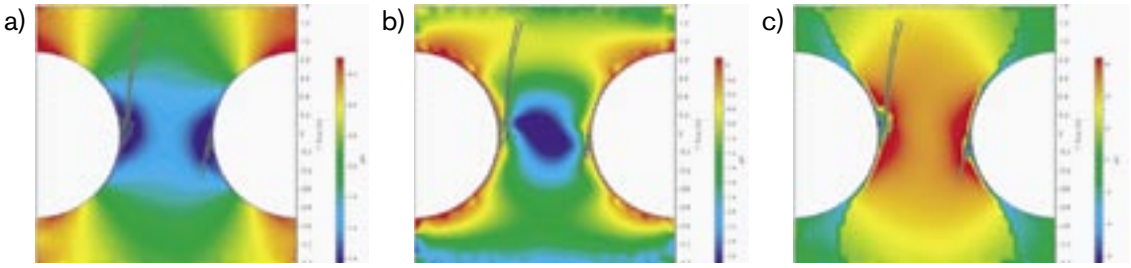

Figure A1-2. *Fracture propagation produced by low K_{IIC}. (a) σ_1 distribution; blue area $\sigma_1 \geq 140$ MPa. (b) σ_3 distribution; blue area $\sigma_3 \geq 26$ MPa. (c) σ_τ; red area $\sigma_\tau \geq 60$ MPa. K_{IIC}=4.40 is valid only in the vicinity of the borehole boundary at low confinement (red area in the middle figure). Asymmetric fracture pattern depends on slight asymmetry in stress distribution due to 3-D effects from the tunnel above and due to confinement at right borehole wall.*

A1.6 Fracture stiffness of new fractures

A1.6.1 Barton-Bandis model

Barton-Bandis model has been used to estimate the normal stiffness of the new fractures. The fracture properties were estimated separately for tensile fracture and shear fractures /Rinne et al. 2003a/. Due to the difference in surface roughness, tensile fractures and shear fractures have different stiffness and dilation values. The estimated normal fracture stiffness was K_n =4,643 (GPa/m) for shear fractures and 320 (GPa/m) for tensile fractures. The current code applies constant K_n once it is determined using the initial JRC values (JRC = 20 for tensile fracture and JRC = 5 for shear fracture). During the previous modelling work the shear stiffness obtained from the Barton-Bandis model was found to be too low for modelling random fracture initiation. The elastic shear deformation was restricted by high stiffness, while only fracture sliding caused shear deformation.

A1.6.2 Laboratory results

According to the recent laboratory tests with artificial fractures of Äspö diorite /Backers, 2003/, the average initial fracture normal stiffness (K_{ni}) is 175 ± 68 GPa/m. It varies between 105 GPa/m and 311 GPa/m at the loading between 0 and 1.5 MPa. At loading between 12 and 25 MPa the average fracture normal stiffness (K_{nh}) is 26,976 ± 22,757 GPa/m. The values are from 2,813 GPa/m to 54,254 GPa/m.

A1.6.3 Calculations

The sensitivity of fracture stiffness of new initiated fractures on failure has been investigated numerically. It must be noted that the artificial fractures that was tested in laboratory are not fully comparable with the new created fractures in the full scale experiment or in models. Newly created fractures in the pillar have a perfect match on their surface and they have not been affected of unloading. The level of normal stress on fracture surface is much higher in the APSE experiment and models compared to laboratory conditions.

A1.6.4 Conclusions

Generally, increasing fracture stiffness of new fractures to a certain level amplifies the failure process for the pillar model. The effect of K_s or K_n seems to be less pronounced when stiffness is more than 5,000 GPa/m. Low stiffness values (< 5,000 GPa/m) seem to prevent extending of newly initiated fractures. In the studied loading configuration the effect of fracture stiffness is more obvious for shear fractures compared to tensile fractures.

Suggested value for fracture normal and shear stiffness is 26,976 GPa/m, which is the average K_n from the laboratory tests at loading between 12 and 25 MPa. This is still quite low level of normal compression compared to the experiment conditions. For simplicity, in the final models we don't make any difference between the stiffness for tensile and shear fractures.

Suggested increase of normal fracture stiffness leads to more extent spalling in the FRACOD pillar model compared to the previous model with stiffness defined by Barton-Bandis model (Figure A1-3).

Reduction of the shear stiffness from restricted deformation to 26,976 GPa/m does not have a major effect on failure pattern.

Table A1-5. Effect of fracture stiffness (new initiated fractures).

Parameter Tensile fractures K_s/K_n Shear fractures K_s/K_n	Changed from Standard Case	Effect compared to the Standard Case. Fracture Initiation (FI), Fracture propagation (FP).
175 / 175 175 / 175	All stiffness values reduced to 175 GPa/m.	No FP.
10e20 / 175 10e20 / 175	K_n reduced to 175 GPa/m.	No FP.
175 / 26,976 175 / 26,976	K_s reduced to 175 GPa/m, K_n increased to 26,976 GPa/m.	No FP.
4,643 / 320 4,643 / 4,643	K_s reduced to 4,643 GPa/m.	Slight decrease in FP.
26,976 / 320 26,976 / 4,643	K_s reduced to 26,976 GPa/m.	Very slight decrease in FP.
10e20 / 320 170 / 4,643	Shear fracture; K_s reduced to 170 GPa/m.	No FP.
10e20 / 320 170 / 170	Shear fracture; $K_s = K_n$ reduced to 170 GPa/m.	No FP even if 120 days stress load applied.
170 / 320 10e20 / 4,643	Tensile fracture; K_s reduced to 170 GPa/m.	Increased FI and FP. Cause high tensional stresses and unstabilities during calculations.
170 / 170 10e20 / 4,643	Tensile fracture; $K_s = K_n$ reduced to 170 GPa/m.	Very slight decrease in FP.
10e20 / 320 10e20 / 4,643	STANDARD CASE	See Figure A1-1 for failure pattern.
4,643 / 4,643 4,643 / 4,643	All stiffness values set to 4,643 GPa/m.	Very slight decrease in FP.
26,976 / 26,976 26,976 / 26,976	All stiffness values set to 26,976 GPa/m.	Slightly increased FP.
10e20 / 26,976 10e20 / 26,976	K_n increased to 26,976 GPa/m.	Slightly increased FP.
54,254 / 54,254 54,254 / 54,254	All fractures stiffness increased to 54,254 GPa/m.	Slightly increased FP.

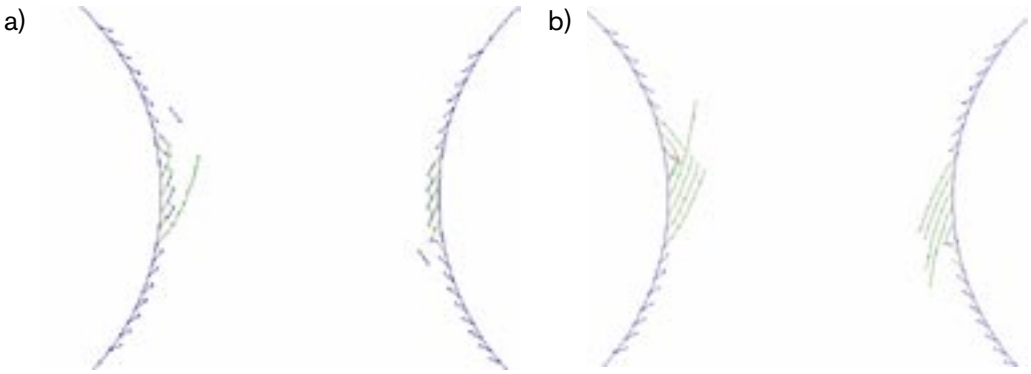

Figure A1-3. *The effect of fracture stiffness. (a) Standard Case. (b) Suggested fractures stiffness.*

The conclusions have been made on limited number of calculations. More in depth analyse of the combined effect of these parameters are suggested. Especially the ratio between K_n/K_s seems to have important role on failure and it should be studied more carefully.

The suggested stiffness values have been tested and checked by numerical UCS simulation (see Figure A1-5.). The results are in line with results from the pillar model.

A1.7 Combined effect of changed material properties

Calculations suggest that the effect of changed parameters increase slightly the area of failure compared to the previous model (compare Figure A1-1b and Figure A1-4b). The impact is not major and the middle part of the pillar remains stable after applying excavation stresses and thermal load of 120 days even in the upper section (0.5 m below tunnel floor).

A1.8 Numerical UCS with suggested parameters

Numerical Uniaxial Compressive Strength tests were made by FRACOD. Results with UCS models are in line with results from laboratory test of Äspö diorite /Kuula, 2003/. Parameters used for the UCS model are presented in Table A1-6. Other parameters are the same as suggested to be applied in the next modelling phase (Table A1-1). Intact rock friction angle (49°) and intact rock cohesion (31 MPa) was used referring to a Uniaxial Compressive Strength of 166 MPa.

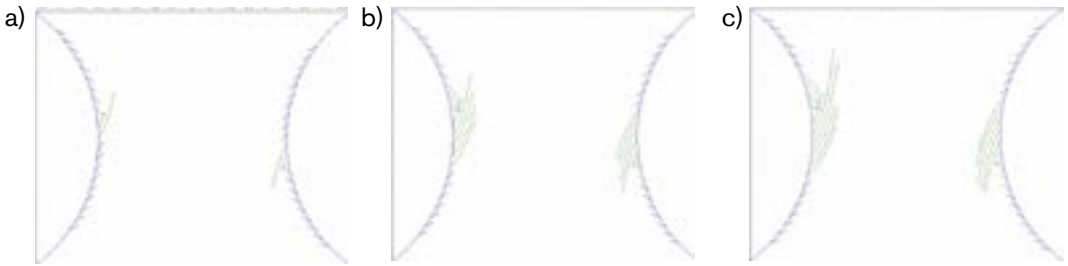

Figure A1-4. *Combined effect of changed parameters for pillar stability. (a) Fracture pattern after excavation, (b) after 30 days after heating and (c) after 120 days heating.*

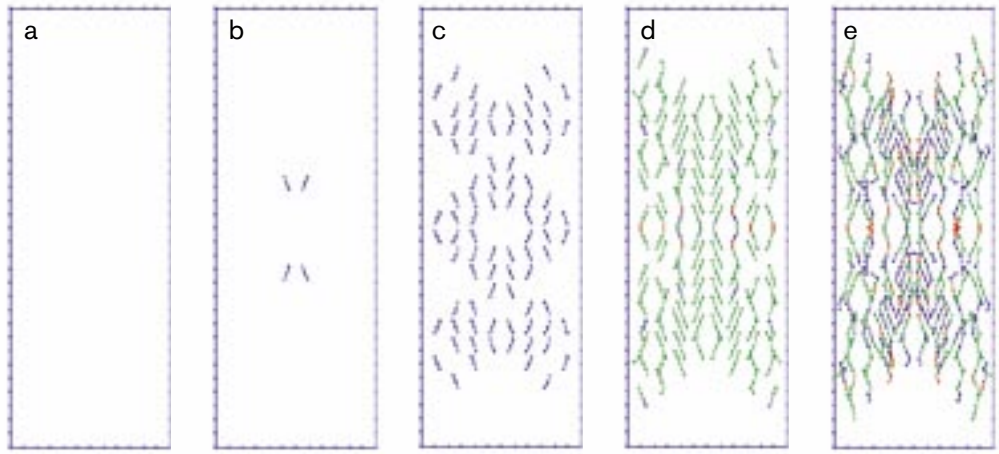

Figure A1-5. *Numerical UCS by FRACOD. Model size 50 mm × 138 mm (a) Load 0 to 120 MPa, results in elastic response. (b–c). Fracture initiation starts at 120 MPa and increase successively with increasing load. (d) Unstabe fracture propagation starts at 170 MPa and leads to failure (e).*

Table A1-6. Input parameters for UCS test.

Poisson s ratio (intact rock)	Young's modulus (intact rock)	KIIC (unconfined loading)	Fracture initiation level
0.25	75.6 GPa	4.40 MPa $m^{1/2}$	121 MPa (76% of UCS)

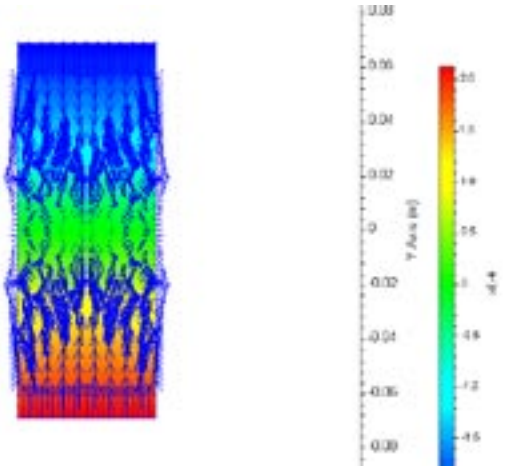

Figure A1-6. *Total axial deformation at start of unstable fracture propagation ≈ 0.4 mm.*

A1.9 Summary of studied parameters

Table A1-7. Significance of parameters on fracturing.

Parameter	Effect compared to the Standard Case
K_{IC}: 2.54=>3.80 MPa $m^{1/2}$	Parameter suggested to be changed. Slight effect of failure.
K_{IIC}: 6.35 MPa $m^{1/2}$	K_{IIC} is proposed to be unchanged for the next modelling phase. Suggested value may slightly underestimate failure at the borehole boundary, and overestimates failure in the pillar.
K_s =K_n= 26,976 GPa/m for both shear and tensile fractures	The suggested increase of normal fracture stiffness leads to more extent spalling. The effect of reducing K_s is insignificant. The sensitivity of K_s and K_n seem not to be critical after reaching a level of >5 000 GPa/m.
σ_t: 14.8→14.3 MPa	Parameter suggested to be changed. However, slight decrease of tensile strength has no effect under proposed loading configuration.
UCS 166 MPa	Intact rock friction angle (φ =49°) and intact rock cohesion (c=31 MPa) was used in the previous phase models and they are suggested to be unchanged.
UCS: 166→130 MPa	Both c and φ are critical for fracture initiation, but also for final failure. The tested reduction of c or φ leads to unstable fracturing in FRACOD models already before heating.
UCS: 166→210 MPa	High friction angle (73°) prevents all fracture propagation. The effect of increased cohesion (39 MPa) is less marked.

References, see main report

Appendix 2

Modelling of fracture development of APSE by FRACOD

Inverse stress reconstruction

Hee-Suk Lee
Fracom Ltd

March 2004

Contents

A2 Inverse stress reconstruction

A2.1 Overview of inverse stress reconstruction

A hybrid approach has been applied for the pillar modelling as shown in Figure A2-1. Outcomes from the application of the approach and the FRACOD for fracturing process development in the pillar are presented as predictive results in terms of stress, displacements and fracture initiation and growth, under the multiple steps of excavation and heating of the in situ heater tests, whose effects is reflected in the derived equivalent boundary tractions used by the FRACOD.

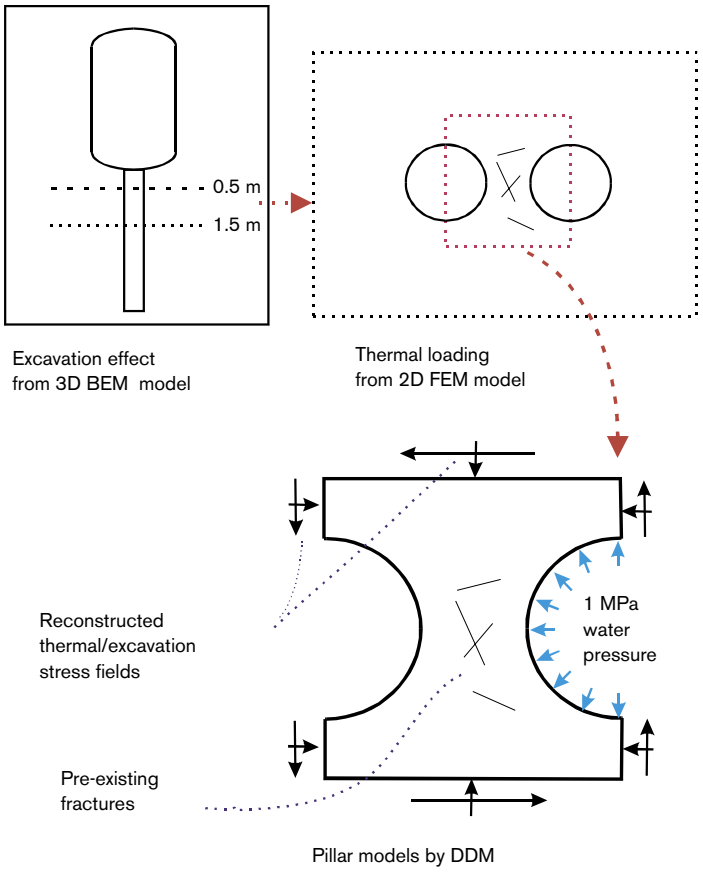

Figure A2-1. *Numerical methods used for the modelling /Rinne et al. 2003a/.*

In this study, a source reconstruction technique was used for our application. If some portion of the boundaries both displacements and tractions are unknown, it cannot be solved directly in a forward boundary value problem senses, because the number of unknowns is larger than number of equations. However, if some quantities, say stresses for our problem at hand, are known at some points inside the domain, the number of the equations can be increased to obtain a solution. Usually the solution of an inverse problem does not always satisfy stability and uniqueness requirements in it self, so it is generally an ill-posed problem. Therefore, special iterative or non-iterative numerical techniques should be applied to get a meaningful solution.

Based on the above concepts, stress distributions from other numerical modelling can be reconstructed after solving unknown boundary tractions with known stress distribution at some points inside the model. The reconstructed tractions along unknown boundaries can be used again to calculate stresses at all other points inside the domain using a conventional BEM code with the calculated boundary tractions directly used as prescribed boundary conditions in a BEM model, without the BEM code to have special functions for domain integral evaluations. A special BEM code was therefore developed to perform just such inversion tasks for this project and the details of the theory and verifications can be seen in /Rinne et al. 2003a/ and /Lee and Jing, 2003/.

A2.2 Pillar model for reconstruction

A2.2.1 Model geometry

To reconstruct the stress field around pillar region, only the pillar region is considered to avoid the thermal sources inside domain like preliminary modelling. Figure A2-2 shows the real test configuration for boreholes and the suggested pillar model for stability analysis. It is noted from comparison, that northern direction of test site corresponds to x-direction of pillar model, and eastern direction in the site is y-direction. All stress data from 3-dimensional orientation has been carefully redefined to 2 dimensional Cartesian coordinate system for reconstruction.

The pillar model cannot be symmetric because the original stress distribution will not be symmetric to the any plane due to 3-D inclined nature. 100 constant BE elements (25 for two arches, 15 for upper and lower edges and 5 for 4 side edges) were used for the pillar model. 479 internal points for known stress distribution were selected as input using recently updated modelling results from previous Examine 3-D by SKB /Andersson, 2003/ and from previous JobFem (thermal stress) by Golder /Fredriksson et al. 2003; Staub et al. 2003/.

A2.2.2 Boundary conditions

- Excavation stage: zero traction around both arches.
- Heating stage: normal traction.
- 0.8 MPa around the right arch to consider backfill (swelling) effects.

To ensure equilibrium in the model, some points should be fixed as zero displacement, but very careful choice of the prescribed points is needed because it affects much the accuracy of the model. We used various combinations of fixed displacements, and concluded zero shear (x-) displacement at the middle of upper and lower edges (0, 1.5 and 0, –1.5) with zero shear (-y) displacement at a mid point one of the arches (–0.5, 0 or 0.5, 0) produced best results.

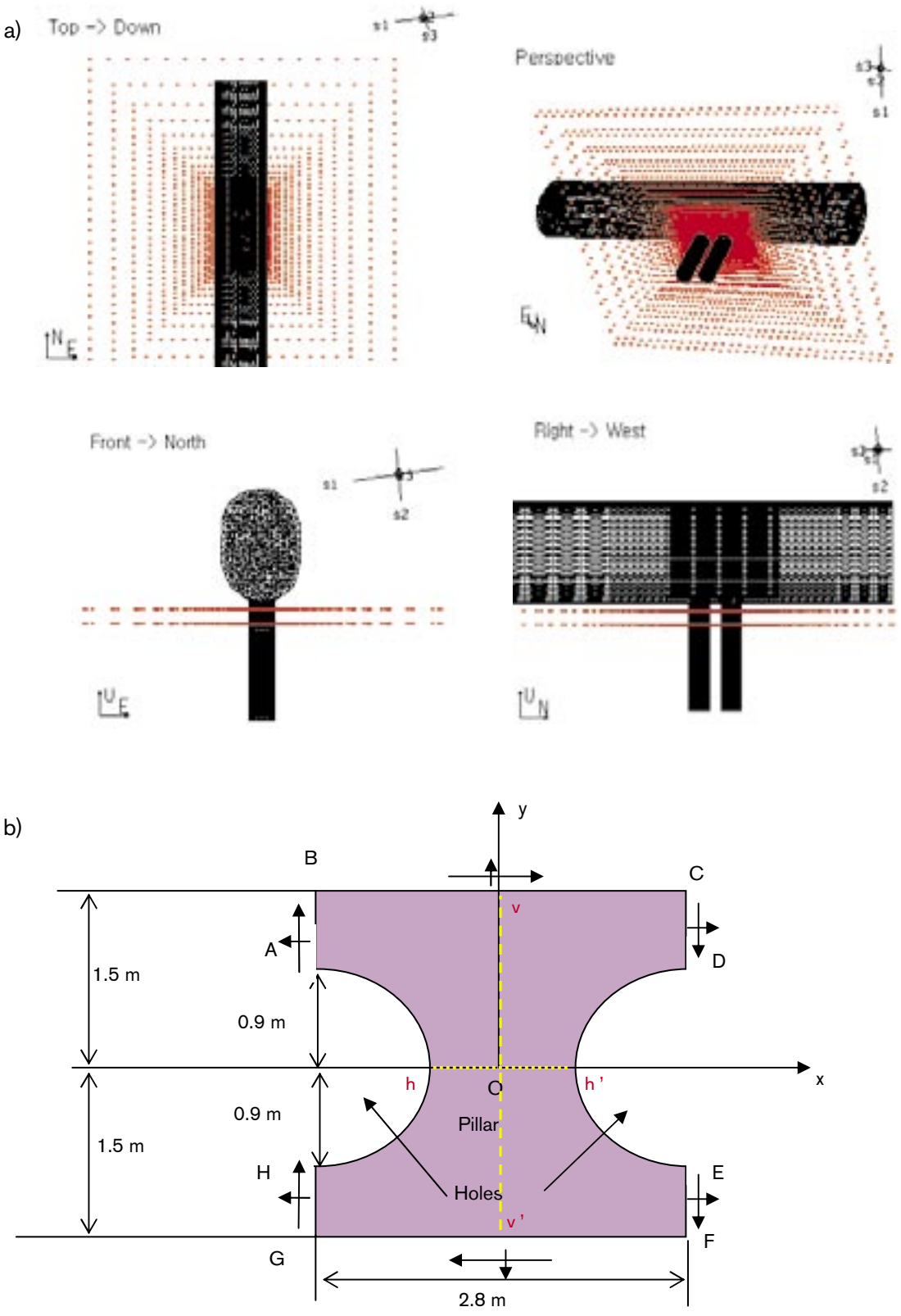

Figure A2-2. *Specification for the pillar model. (a) Real test configuration (b) The Pillar model.*

Main unknown tractions to be solved by inverse analysis were 50 elements along AB-BC-CD and EF-FG-GH sections. Using each set of stress data, stress field was reconstructed using forward analysis with the obtained unknown tractions.

Newly characterised APSE parameters for rock mass (E=55 GPa and ν =0.26). All other properties such as thermal properties will not be needed for the inverse analysis because all thermal effects are preserved in the stress distribution. The effect of 3-D inclined far-field stress is also included in the stress distribution.

Stress distribution after excavation of boreholes is reconstructed at both 1.5 m and 0.5 m depth below the tunnel floor, respectively. Four stages of thermal stress distribution are reconstructed from after 30 days, 60 days, 90 days and 120 days of heating, respectively. All reconstructed data have been converted to FRACOD input to model fracturing behaviour around pillar at each loading.

A2.3 Reconstructed stress field after excavation

Figure A2-3 shows the comparison between original and the reproduced stress field for excavation at 1.5 m below the tunnel floor. It should be noted that all contours are from interpolation of stresses at internal points as shown in Figure A2-3. The reproduced stresses show good agreement for both major and minor principal stresses.

Some differences near middle of holes were detected in the case of minor principal stresses from the preliminary results. This might be mainly due to the degree of mesh refinement and the effect of interpolation with only internal stress data. When FRACOD is used with converted input, smoother distribution could be obtained compared with interpolated distribution. It is also expected that more refined boundary element can solve this problem.

All the reconstructed values were quite similar for both major and minor principal stresses. Small differences less than one percent will not affect the overall accuracy of the FRACOD model. For all truncated numbers, the reproduced results show similar accuracy in the case of 1.5 m below tunnel floor. It is because the singularity of the inverse problem could be diminished by using lots of input stress points.

In the case of reproduced stress field for excavation at 0.5 m below the tunnel floor, accuracy for this depth was quite lower than stress of 1.5 m below the tunnel floor. However, overall reproduced stress distribution is quite similar with the original one. Distance from tunnel floor is just 0.5 m, so the original stress distribution from 3D model must have affected by full 3-dimensional effects. It causes more numerical singularity to the models, so the results showed much discrepancy between original and reconstructed distribution.

More treatment should be needed to consider properly the effect of 3-dimensional stress distributions in the future. Nevertheless, this reproduced stress can also be used for the FRACOD simulation because overall trend and maximum stress values of the reproduced one were very similar to those of the original one, and basic stress pattern is same.

The detailed comparison along horizontal and vertical lines from pillar center is shown in Figure A2-4, and absolute error and residual squares between two distributions are listed in Table A2-1. All points are on the two lines v–v’ and h–h’ as shown in Figure A2-2b (point O is origin). Overall accuracy is quite good even with coarse boundary element mesh for reconstruction in the case of 1.5 m plane. However, the region quite close to the boundary, discrepancy occurred especially in the case of minor stresses.

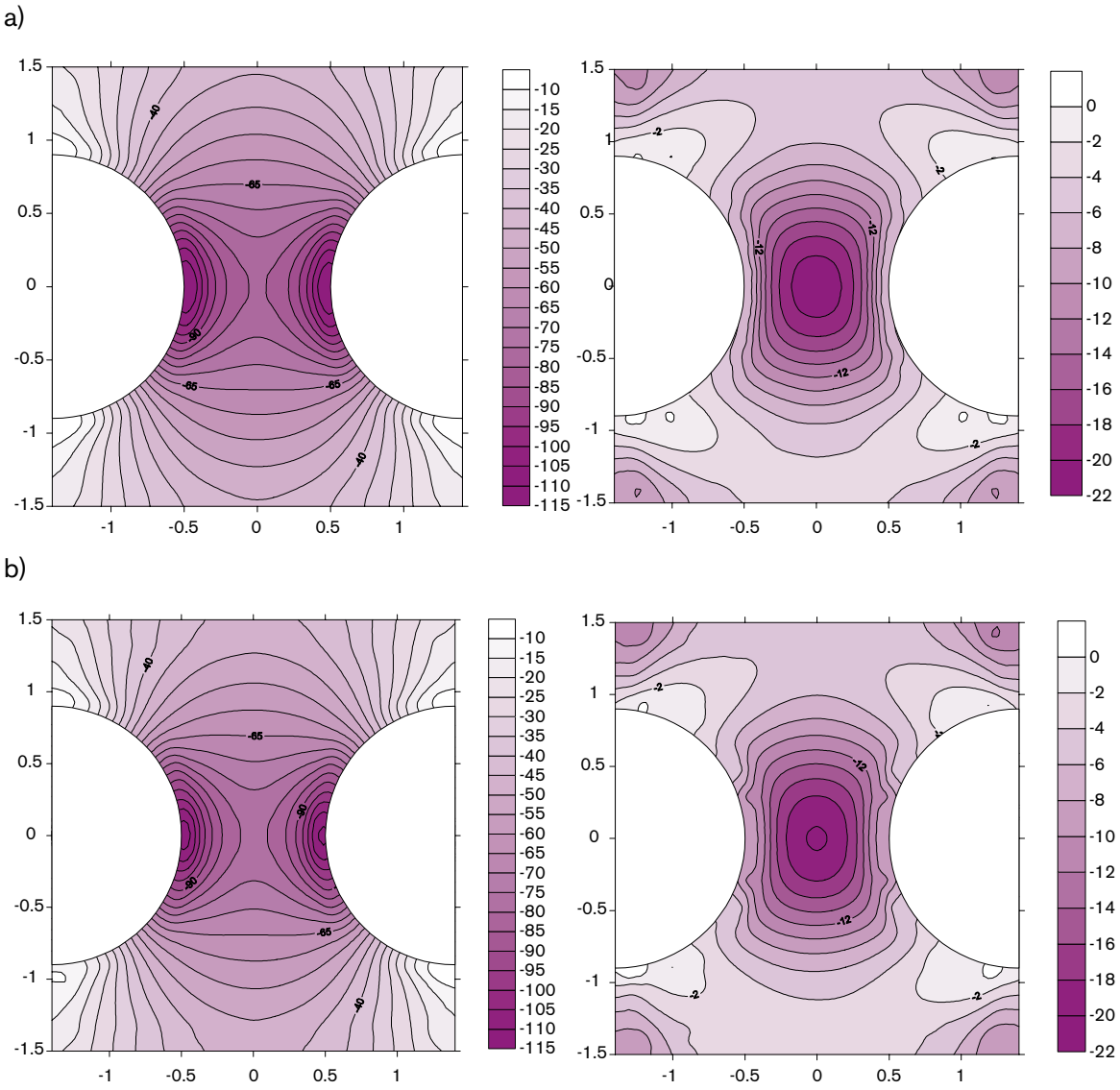

Figure A2-3. *Comparison between the original and the reproduced stress distribution for excavation at 1.5 m below the tunnel floor (left: major principal stress, right: minor principal stress) (a) original distribution (b) reconstructed distribution.*

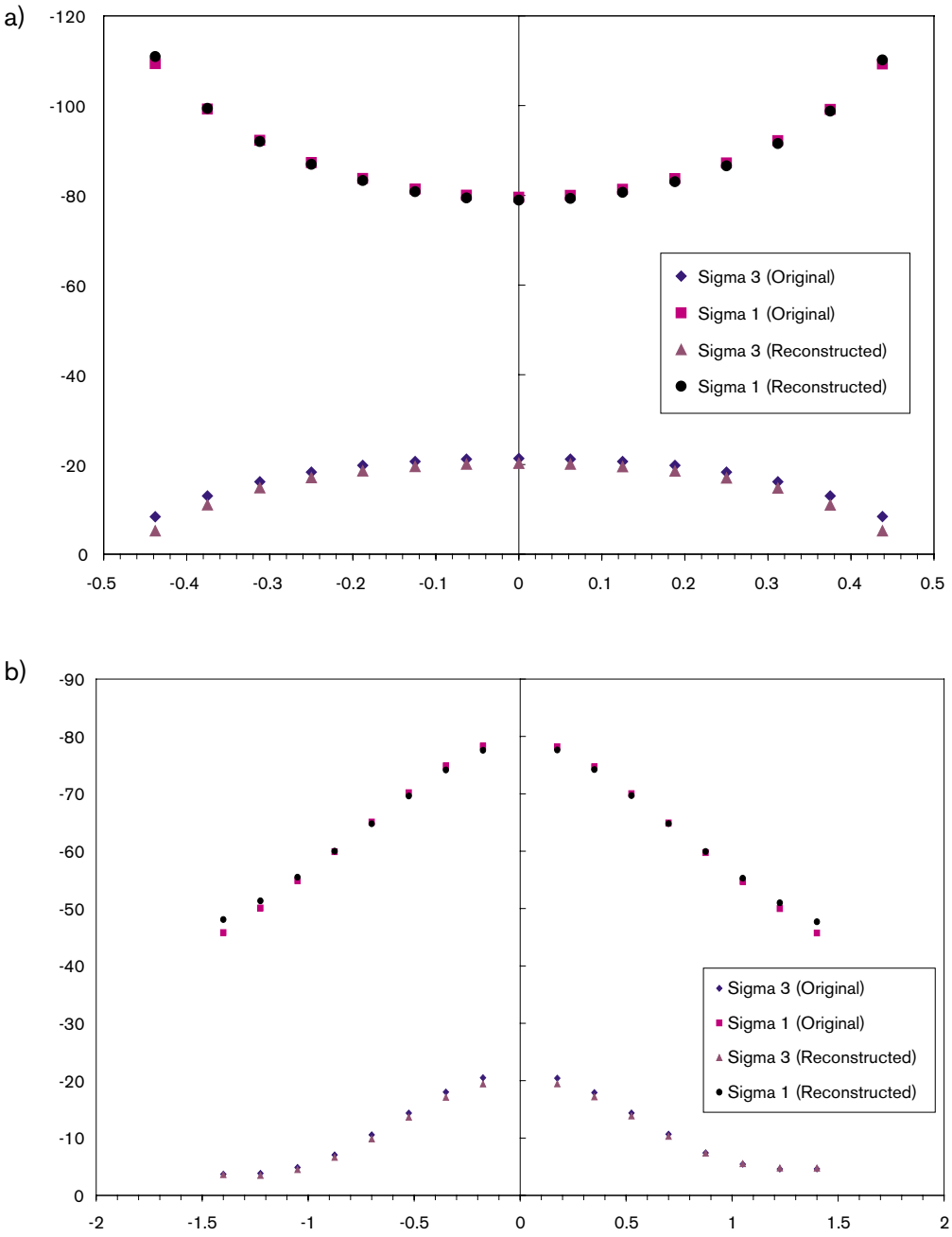

Figure A2-4. *Comparison of the stresses along horizontal and vertical sections inside pillar at 1.5 m below the tunnel floor. (a) Horizontal section (along h–h' line in Figure A2-2b) (b) Vertical section (along v–v' line in Figure A2-2b).*

Table A2-1. Comparison of relative errors and residual squares at several points after excavation.

L	y-	1.5 m Relative Error		Residual Square		0.5 m Relative Error		Residual Square	
0	0	–0.815	–5.210	0.420	1.237	–4.943	–5.111	23.364	1.510
0.125	0	–0.829	–5.677	0.455	1.378	–4.925	–5.954	24.203	1.943
0.25	0	–0.758	–7.051	0.437	1.661	–4.778	–8.299	26.071	3.033
0.312	0	–0.677	–8.819	0.389	2.025	–4.681	–10.673	27.884	3.983
0.438	0	0.819	–38.055	0.800	10.244	–3.419	–84.890	20.864	71.018
0	0.175	–0.721	–4.816	0.318	0.968	–4.115	–3.993	15.624	0.835
0	0.525	–0.479	–3.546	0.112	0.259	–3.770	–4.532	10.197	0.495
0	0.7	–0.197	–3.391	0.016	0.131	–3.143	–8.800	5.891	0.998
0	1.05	1.032	1.637	0.319	0.008	3.149	–18.500	3.881	1.090
0	1.4	4.297	3.181	3.862	0.022	13.498	–10.470	45.920	0.242

As shown in above comparison in the case of 0.5 m below tunnel floor, 3-dimensional stress distributions cannot be fully reconstructed with 2-dimensional inverse model because of out of plane stresses. However, for practical use, obtained stress pattern can be applied for 2D fracturing model because maximum stress level and stress pattern is similar. Other solution strategy including consideration of full 3-D stress reconstruction should be sought to get the exactly same distribution.

A2.4 Reconstructed stress field after heating

Thermal stresses calculated by JobFem with updated properties and final heating condition, were reproduced with inverse model for the pillar model. Figure A2-5 shows a comparison between the original and the reproduced stress distribution for both major and minor principal stresses after 120 days of heating.

All results are from regular SVD solution without truncation, because the accuracy of the stress field was quite similar for all truncation numbers. Compared with the excavation effect, better accuracy between two models could be obtained for both major and minor principal stresses. The reproduced stress distribution showed excellent agreement with the original one except a point near central boundary. This problem is also due to mesh refinement and singularity of BEM formulation.

Table A2-2 lists relative errors and residual squares at some selected points inside pillar. All points are on the two lines v–v' and h–h' as shown in Figure A2-2b (point O is origin). In the case of major principal stress, reconstructed distribution show good agreement with original distribution at each loading steps. In most cases, errors for the major principal stress show below 1%. Errors were quite small especially in the case of thermal stresses compare to the case of excavation. Errors for minor stress seem to be quite large when relative errors are calculated due to original small values. However, residual squares are quite small, thus real differences can be accepted for FRACOD model. When finer mesh is used around the pillar for FRACOD input, these discrepancies can be minimized.

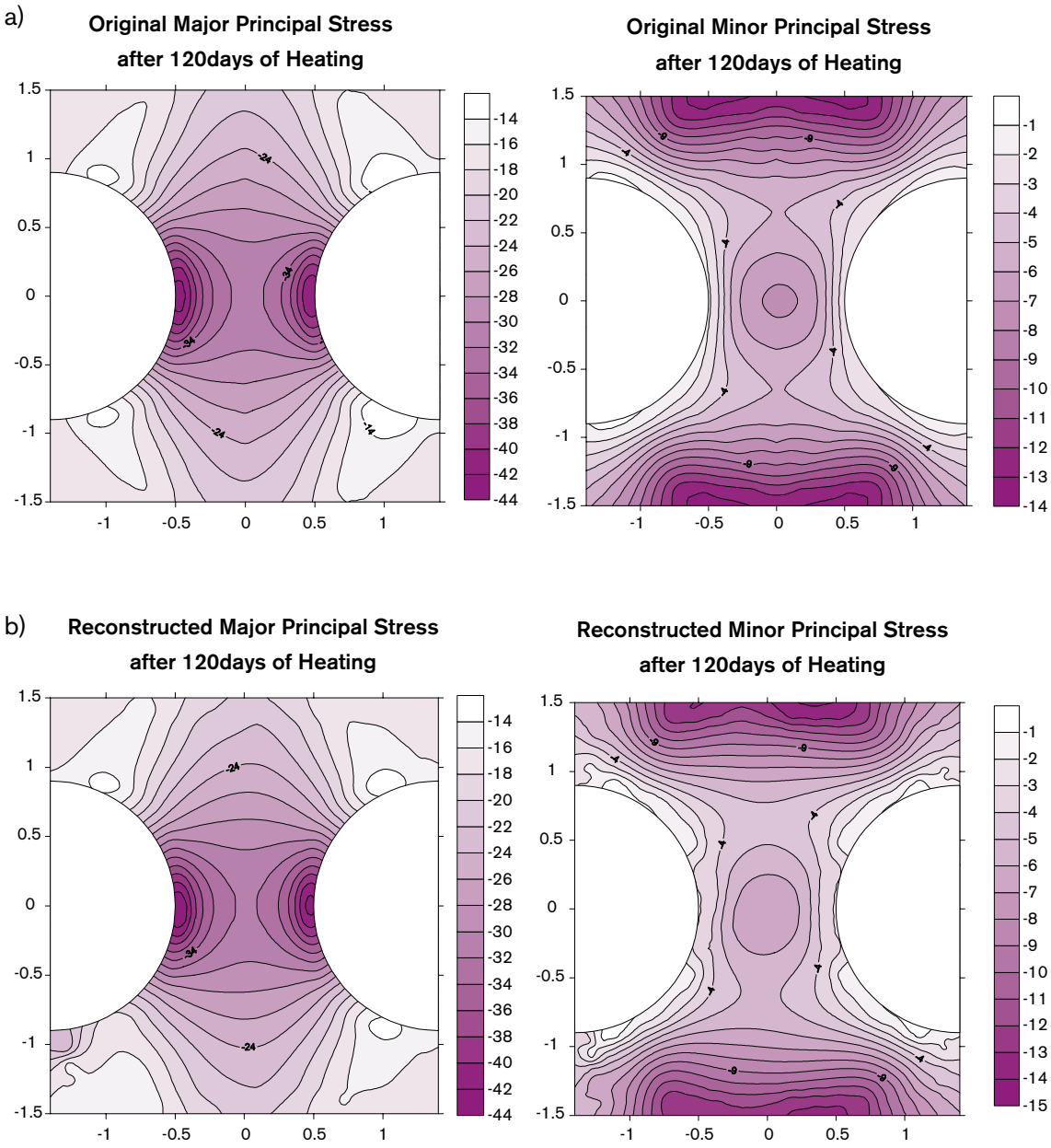

Figure A2-5. *Comparison between the original and the reproduced stress distribution after 120 days of heating (left: major principal, right: minor principal stress) (a) original distribution (b)reconstructed distribution.*

Table A2-2. Comparison of relative errors and residual squares at several points after heating.

(x,y coord.)			0,0	0.125,0	0.25, 0	0.312, 0	0, 0.175	0, 0.525	0, 0.875	0, 1.125	0, 1.4
30 day	**R.E.***	σ_1	1.856	1.986	1.781	1.456	1.621	0.286	–1.340	–3.147	–2.716
		σ_3	–9.828	–13.554	–18.816	–22.744	–12.593	–32.807	–6.365	4.393	–0.663
	R.S.**	σ_1	0.083	0.095	0.084	0.062	0.063	0.002	0.037	0.177	0.122
		σ_3	0.104	0.201	0.362	0.467	0.135	0.109	0.001	0.017	0.001
60 day	**R.E.**	σ_1	1.233	1.324	1.231	1.032	1.027	–0.198	–1.553	–2.876	–3.007
		σ_3	–6.715	–9.342	–13.411	–16.626	–8.862	–13.248	–1.853	3.396	1.691
	R.S.	σ_1	0.077	0.090	0.087	0.067	0.053	0.002	0.091	0.256	0.253
		σ_3	0.112	0.214	0.388	0.502	0.168	0.140	0.002	0.036	0.018
90 day	**R.E.**	σ_1	0.988	1.127	1.127	1.000	0.798	–0.395	–1.635	–2.729	–3.109
		σ_3	–5.764	–7.760	–11.071	–13.794	–8.009	–10.220	–1.292	3.416	2.710
	R.S.	σ_1	0.074	0.098	0.110	0.095	0.047	0.010	0.141	0.315	0.366
		σ_3	0.128	0.227	0.395	0.507	0.220	0.181	0.003	0.067	0.074
120 day	**R.E.**	σ_1	0.927	0.984	0.917	0.764	0.737	–0.440	–1.660	–2.688	–3.247
		σ_3	–5.033	–6.949	–10.124	–12.734	–6.965	–8.149	–0.947	2.890	2.477
	R.S.	σ_1	0.085	0.099	0.096	0.073	0.053	0.016	0.184	0.380	0.494
		σ_3	0.131	0.243	0.434	0.561	0.227	0.183	0.003	0.071	0.085

* Relative Error.

** Residual Square.

A2.5 Concluding remarks

Stress distribution from updated properties and test condition inside the pillar has been successfully reconstructed with the developed inverse BEM technique. Concluding remarks from reconstruction can be summarized as follows:

Overall stress distribution with the suggested pillar model could be well reproduced with allowable accuracy by the inverse reconstruction method. Some discrepancy has occurred in the vicinity of the boundaries. It is expected that this problem can be minimized when the inputs are applied to FRACOD. Limitation from reconstructed distribution at 0.5 m below tunnel floor requires 3-D inverse reconstruction or direct consideration of excavation and thermal loading FRACOD itself.

Because reconstructed distribution is from an elastic model without any fractures, uncertainties are involved for the model itself. However, the obtained stress distribution can be applied for modelling current APSE experiment with FRACOD model.

References, see main report